



This is a repository copy of *Accelerated carbonation of reactive MgO and Portland cement blends under flowing CO₂ gas*.

White Rose Research Online URL for this paper:

<https://eprints.whiterose.ac.uk/id/eprint/157828/>

Version: Accepted Version

Article:

Wang, L., Chen, L., Provis, J.L. orcid.org/0000-0003-3372-8922 et al. (2 more authors) (2020) Accelerated carbonation of reactive MgO and Portland cement blends under flowing CO₂ gas. *Cement and Concrete Composites*, 106. 103489. ISSN 0958-9465

<https://doi.org/10.1016/j.cemconcomp.2019.103489>

Article available under the terms of the CC-BY-NC-ND licence
(<https://creativecommons.org/licenses/by-nc-nd/4.0/>).

Reuse

This article is distributed under the terms of the Creative Commons Attribution-NonCommercial-NoDerivs (CC BY-NC-ND) licence. This licence only allows you to download this work and share it with others as long as you credit the authors, but you can't change the article in any way or use it commercially. More information and the full terms of the licence here: <https://creativecommons.org/licenses/>

Takedown

If you consider content in White Rose Research Online to be in breach of UK law, please notify us by emailing eprints@whiterose.ac.uk including the URL of the record and the reason for the withdrawal request.



eprints@whiterose.ac.uk
<https://eprints.whiterose.ac.uk/>

Accelerated Carbonation of Reactive MgO and Portland Cement Blends Under Flowing CO₂ Gas

Lei Wang^{1,2}, Liang Chen¹, John L. Provis², Daniel C.W. Tsang^{1,*}, Chi Sun Poon¹

¹ Department of Civil and Environmental Engineering, The Hong Kong Polytechnic University, Hung Hom, Kowloon, Hong Kong, China.

² Department of Materials Science and Engineering, The University of Sheffield, Sir Robert Hadfield Building, Mappin St, Sheffield S1 3JD, United Kingdom.

* Corresponding author: dan.tsang@polyu.edu.hk

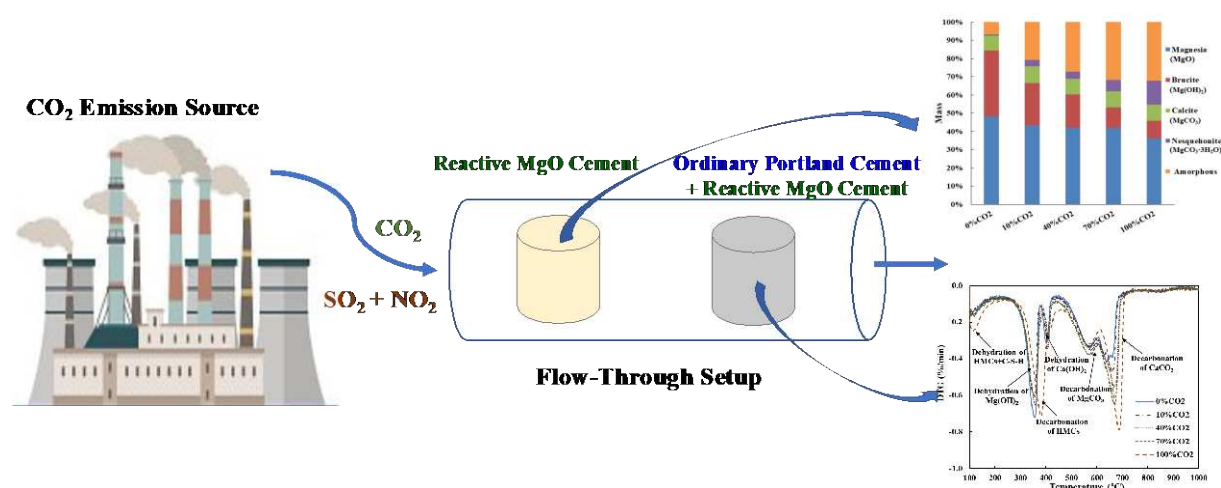
Abstract

The use of MgO-based materials for sequestration of CO₂ offers technical advantages and environmental incentives. However, the understanding of accelerated carbonation of MgO-based materials in flowing CO₂ gas is limited. This study elucidates the carbonation behaviour of reactive MgO cement (MC) and MgO-Portland binary cement (BC) in a simulated CO₂-rich industrial exhaust. Quantitative X-ray diffraction and thermogravimetric analyses showed that nesquehonite (MgCO₃·3H₂O) was the major carbonation product in MC pastes, whereas CaCO₃ was preferentially generated in BC pastes. The relative humidity of exhaust gas influenced CO₂ diffusion and the carbonation rate; 98% humidity facilitated MC carbonation whereas 50% was favourable for BC carbonation. Although CO₂ concentration determined the carbonation rate, 10% CO₂ gas in the exhaust was sufficient to accelerate carbonation. The carbonation degree and compressive strength of samples cured for 7 days at 10% CO₂ were comparable to the values of samples cured for 1 day at 100% CO₂. The presence of acid gases during CO₂ curing inhibited the carbonation and hydration processes, but the presence of Portland cement in the BC system gave good compatibility with acids and relieved the inhibitory effect. Desulphurization and denitrification of industrial exhaust gas are nonetheless

desirable before CO₂ curing. This study builds the foundation for utilising industrial CO₂ exhaust to accelerate the carbonation of Mg-based materials.

Keywords: eco-friendly cement; CO₂ sequestration/utilisation; amorphous hydrated carbonate; cement hydration chemistry; gaseous waste valorisation; sustainable chemistry/engineering.

Graphical Abstract



Highlights:

- MgO-based cement can sequester and utilize CO₂ from industrial exhaust.
- Relative humidity influenced CO₂ diffusion and carbonation rate.
- 7-d curing with 10% CO₂ concentration ensured sufficient carbonation degree.
- Acid gases in exhaust severely inhibited carbonation and hydration.
- Binary MgO-Portland cement showed fast carbonation rate and good compatibility with acids.

1. Introduction

Cement and concrete have been essential materials for the urbanisation of society. More than 10 billion tonnes of concrete are annually generated worldwide, which has been the second-most-used material in the world only behind water [1]. Concrete is usually based on ordinary

Portland cement (PC) as a binding material, due to its robust, reliable, and inexpensive nature. PC is generated from calcination of limestone and clay minerals at 1400 °C in a kiln, which is associated with a high CO₂ emission (660–820 kg CO₂ per tonne) contributing to approximately 7-10% of global anthropogenic CO₂ emissions [2-4]. Therefore, extensive research has been devoted to developing alternative low-carbon cementitious systems to partially or totally replace PC in certain applications.

Reactive magnesia cement (MC) is a promising candidate “green cement”, produced by the calcination of magnesite at relatively low temperature (650–800 °C) [5,6]. Recently, recovery of Mg²⁺ from salt lakes and seawater to produce MC has been proposed as an eco-friendly approach [7], as the low geological abundance of high-purity magnesium minerals in many parts of the world constrains the uptake of magnesia-based cements [8]. However, in locations where suitable resources are available at scale, this is a potentially attractive route to valorisation of under-utilised resources. For instance, as a by-product of the Li₂CO₃ production from salt lakes, there are 200,000 tonnes of MgO produced annually in Qarhan Salt Lake in Qinghai Province, China [9]. Partial MC replacement in PC-based cementitious binder systems could enhance the properties of cement and concrete products, including characteristics such as denser pore structure, higher mechanical strength, superior resistance to chemical attack and corrosion, as well as excellent compatibility with contaminants [10,11].

Recent research has shown that MC is a versatile material that can be used alone as a binder, or blended with other materials for diverse applications, such as MgO expansive cements, MgO-based self-healing materials, MgO-based stabilization/solidification agents, MgO-modified alkali-activated materials, magnesium phosphate cements, magnesium oxychloride (Sorel) cements, magnesium oxysulphate cements, magnesium silicate hydrate (M-S-H)

cements, and others [8,12,13]. Importantly, MC derived from an efficiently-produced magnesite source is regarded by some as a “carbon negative” cementitious material, as it can sequester CO₂ and gain improved binding properties during accelerated carbonation [14,15]. CO₂ curing has been suggested to accelerate the carbonation of cement-based products and facilitate carbon sequestration in solid mineral phases [16,17]. During CO₂ curing, dissolved and ionised CO₂ induces the carbonation of Ca²⁺/Mg²⁺ ions from the cement matrix, which then precipitates in the voids of the matrix as carbonates (anhydrous and hydrated) in a short period of time, boosting setting and hardening process, forming a dense, strong and potentially stable structure [18-20]. MC usually contains more than 85% active MgO, and the CO₂ sequestration capacity can reach up to 92.8 wt%, which is higher than the capacity of PC (50.4 wt%) based on theoretical calculation. The carbonation of MC can take place via the formation of magnesium carbonate (MgCO₃) from hydrated Mg(OH)₂ by the uptake of CO₂:



or with the incorporation of water to form hydrated magnesium carbonates (HMCs), including nesquehonite (MgCO₃·3H₂O), dypingite (Mg₅(CO₃)₄(OH)₂·5H₂O), and artinite (Mg₂(OH)₂CO₃·3H₂O). In most cases, nesquehonite is the most prominent Mg carbonate phase during CO₂ curing:



HMCs can form a well-densified structure with good binding ability, thus enhancing the mechanical properties of MC-based products [8,21]. The reaction pathways and quantitative compositions of HMCs are kinetically and thermodynamically controlled by many factors such as temperature, CO₂ pressure, ionic strength, etc [22, 23].

Accelerated carbonation of MC is well documented in the recent literature [24,25]. However, most of these studies have reported accelerated carbonation that was performed in a static CO₂

curing chamber with pressured and concentrated CO₂ gas [26,27]. This static CO₂ curing can make the maximum use of CO₂ for accelerated carbonation and facilitate the investigation of the mechanisms of MC carbonation. However, some researchers have pointed out that the static CO₂ curing represents an ideal CO₂ curing, which is an energy-intensive approach and far from practical application [28]. As the carbonation of MC is rate-limited and quite slow in an atmospheric environment, it has been argued that the re-adsorption of CO₂ from the environment will not take place to a meaningful extent in MC during its service life, meaning that the classification of “carbon negative” is doubtful [8]. The carbonation of MC and PC binary system has attracted wide attention, because the binary cement could utilise their respective advantages and alleviate individual drawbacks, achieving satisfactory carbonation efficiency, early strength, and durability [27,29]. Up to now, there is no consensus that MC and MC-based cementitious materials can be effectively carbonated to sequester CO₂ in practical situations.

In this study, we investigate the potential efficacy of accelerated carbonation of MC and MgO-based binary cement (BC) in a field-relevant situation. The flow-through CO₂ curing system can simulate a real process exhaust situation, which allows adjustable temperature, humidity, flow rate, and CO₂ concentration. The flow-through curing system can utilise CO₂-rich industrial exhaust gas as a CO₂ source for carbonation, e.g., flue gases from fossil-fuel power plants, cement rotary kilns, steelworks, and refuse incineration plants, which may contain CO₂ concentrations ranging from 5% to 20% [30]. Because the carbonation rate is sensitive to exposure conditions during CO₂ curing [31], the effects of parameters in the exhaust gas supply (CO₂ concentration, relative humidity) on carbonation of MC and BC are investigated. Additionally, exhaust CO₂ gas is usually associated with acid gases (such as SO₂ and NO₂), which should be considered before practical applications, so these contaminants are included

in the gas environment for selected experiments.

To explore the carbonation efficiency of MgO-based cement in simulated industrial exhaust gases, this study aims to: (i) assess the effect of relative humidity on the CO₂ diffusion and carbonation of MgO pastes; (ii) elucidate the influence of CO₂ concentration on the carbonation rate and formation of final carbonates; (iii) evaluate the interference of acid gases with the accelerated carbonation of MgO systems; and (iv) investigate the interactions between MC and PC in the flow-through CO₂ curing system.

2. Materials and Methodology

2.1 Materials and Sample Preparation

Reactive MgO cement and ASTM Type I ordinary Portland cement were used in this study. The MC with a density of 3.15 g cm⁻³, produced from the calcination of MgCO₃ at 700 °C, was obtained from Renheng Magnesium Company, Liaoning Province, China. The PC with a density of 3.16 g cm⁻³ was purchased from Green Island Cement Limited, Hong Kong. The chemical compositions of the PC and MC cement were determined by X-ray fluorescence (XRF) and are listed in Table 1. The particle size distribution and the X-ray diffraction (XRD) data obtained for PC and MC are presented in Figure S1 and Figure S2 (Supplementary Information). Reagent-grade Mg(NO₃)₂, NaCl, and K₂SO₄ used for adjusting the relative humidity were purchased from Tianjin Chemical Reagent Factory, China. Reagent-grade H₂SO₄ (95-98%) and HNO₃ (70%) solution for simulating acid gases were purchased from Sigma-Aldrich.

The MC binder and a binary cement (BC) binder were investigated in the flow-through CO₂ curing condition. The BC binder was composed of 50 wt% MC and 50 wt% PC. The water-to-

binder ratio was kept at 0.25 in both cases, giving zero slump paste mixtures, which was advantageous for block production and subsequent CO₂ curing [29]. To simulate the interference of acid gases (SO₂ and NO₂), H₂SO₄ (0.125 wt% of paste) and HNO₃ (0.0137 wt% of paste) were added into specified mixtures based on theoretical calculation (in Supplementary Information). For the production of MC and BC blocks, water was added into the binder and mixed for 3 min by a planetary stirrer. The fresh pastes were cast in steel cylindrical moulds (55 mm internal diameter) and compacted with 30 MPa pressure until the height of the sample was compressed to 55 mm. After an additional 1 min compaction, the samples were demoulded immediately without slump and subjected to different curing conditions. In the flow-through CO₂ curing chamber, the relative humidity of gas was controlled at 50%, 75%, and 98% by equilibration with saturated Mg(NO₃)₂, NaCl, and K₂SO₄ solutions respectively; the CO₂ concentration was adjusted to 0%, 10%, 40%, 70%, and 100%; the curing times (i.e., periods of CO₂ curing) were 6 h, 1 d, 3 d, and 7 d. All experiments were conducted in triplicate and the average values are reported with error bars where appropriate. The CO₂ concentration was adjusted by controlling the blending ratio of variable flow rates of air and CO₂ gas, and a CO₂ meter (CM-0003, CO₂Meter) was used to monitor and record the CO₂ concentration in the flowing gas. A schematic diagram of the flow-through CO₂ curing set up is shown in **Figure 1**.

Table 1. Chemical compositions of PC and MC (wt %)

	Na ₂ O	MgO	Al ₂ O ₃	SiO ₂	P ₂ O ₅	SO ₃	K ₂ O	CaO	Fe ₂ O ₃	LOI
<i>PC</i>	0.17	1.38	4.79	18.99	0.08	4.52	0.79	65.72	3.10	2.45
<i>MC</i>	0.00	90.46	0.46	5.81	0.10	0.10	0.15	2.22	0.59	5.42

LOI: loss on ignition; PC: ordinary Portland cement; MC: reactive MgO cement.

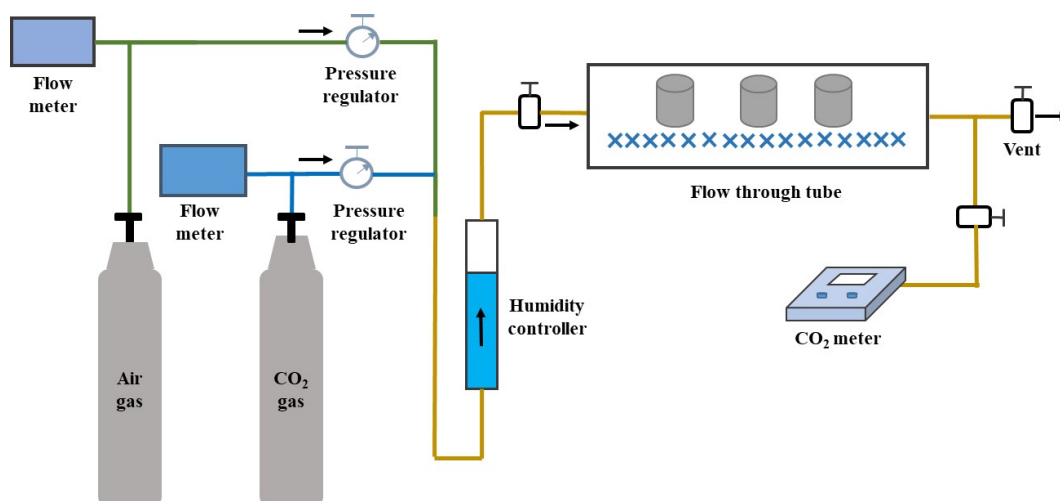


Figure 1. Schematic diagram of flow-through CO₂ curing setup.

2.2 Physical Properties and Thermogravimetric/Spectroscopic/Microscopic Analyses

The uniaxial compressive strength of the MC and BC blocks was examined by using a standard testing machine (Testometric CXM 500-50 KN) at a loading rate of 0.6 MPa s⁻¹ [32]. Thermogravimetric analysis (TGA) of powder samples was performed by heating from 40°C to 1000 °C at 10 °C min⁻¹ with argon purge gas (Rigaku Thermo Plus). Crystalline-phase mineralogy of samples was determined using a high-resolution powdered X-ray diffractometer (XRD, Rigaku SmartLab) in the range $2\theta = 15\text{-}45^\circ$ at a rate of 3° min⁻¹, with Cu K α adiation generated at 45 kV and 200 mA. It should be noted that the XRD scan at a low angle is also important for detecting the strong peaks of hydrated magnesium carbonates in this range. For quantitative X-ray diffraction (Q-XRD) analysis, 20 wt% corundum (Al₂O₃) was used as an internal standard to determine the content of amorphous constituents, although it was regarded as a semi-quantitative method in view of the likelihood of errors. The Q-XRD analysis was calculated by the whole powder pattern fitting (WPPF) method of the integrated X-ray powder diffraction software (PDXL). The surface morphology and elemental distribution of samples with Au coating were investigated by scanning electron microscopy with energy-dispersive X-ray spectroscopy (SEM-EDX, TESCAN VEGA3 XM) at an accelerating voltage of 15 kV with

a current of 70-78 μA . For quality assurance, all of the samples were crushed into specified size and homogeneously mixed for the analytical tests.

3. Results and Discussion

3.1 The Role of Relative Humidity in Hydration and Carbonation

3.1.1 MC Pastes

From the thermogravimetry (TG) curves (Figure 2a), the weight loss from 100 °C to 300 °C can be ascribed to the evaporation of the physically adsorbed water and bound water from the hydrated magnesium carbonates (HMCs, e.g. nesquehonite) [27]. The sharp peaks near 370 °C and 390 °C in the derivative thermogravimetry (DTG) curves (Figure 2b) correspond to the dehydroxylation of $\text{Mg}(\text{OH})_2$ and decarbonisation of HMCs, respectively [27]. The mass drop at higher temperatures (from 500 °C to 600 °C) was associated with the decomposition of metastable Mg-carbonates. The peaks at temperatures above 600 °C mainly result from the decomposition of stable, well-crystallized MgCO_3 [23]. In the 1-d air cured samples, there was a mass loss of 12.3 wt% at 370 °C (Figure 2a), equivalent to 39.7 wt% $\text{Mg}(\text{OH})_2$ content. The air cured samples also showed 4.32 wt% mass loss due to carbonates (equivalent to 8.25 wt% MgCO_3), which resulted from the original MgCO_3 in raw MgO cement (Figure S2). By comparison, after 1-d CO_2 curing, the $\text{Mg}(\text{OH})_2$ peak was reduced and shifted from 370 °C to 390 °C, especially in the samples with 98% humidity CO_2 curing. An obvious dehydration peak of HMCs could be observed in the 98% humidity samples. Thus, 98% humidity was selected as the optimal humidity for the carbonation of MC samples, although 50% humidity was regarded as an optimal humidity for PC system in a previous study [16]. This is attributed to the relatively high water consumption for the dissolution of $\text{Mg}(\text{OH})_2$ ($K_{\text{sp}} = 1.13 \times 10^{-11}$ at 25 °C) compared to the $\text{Ca}(\text{OH})_2$ ($K_{\text{sp}} = 5.02 \times 10^{-6}$ at 25 °C) resulting from Portland cement hydration [33]. It should be noted that the content of MgCO_3 (approximately 10.32%) was

similar in all 1-d samples. This suggests that $\text{Mg}(\text{OH})_2$ was preferentially carbonated into HMCs [34], because the ΔG of $\text{MgCO}_3 \cdot 3\text{H}_2\text{O}$ generation ($-38.7 \text{ kJ mol}^{-1}$) was lower than the energy of MgCO_3 generation ($-30.2 \text{ kJ mol}^{-1}$) (Figure S3).

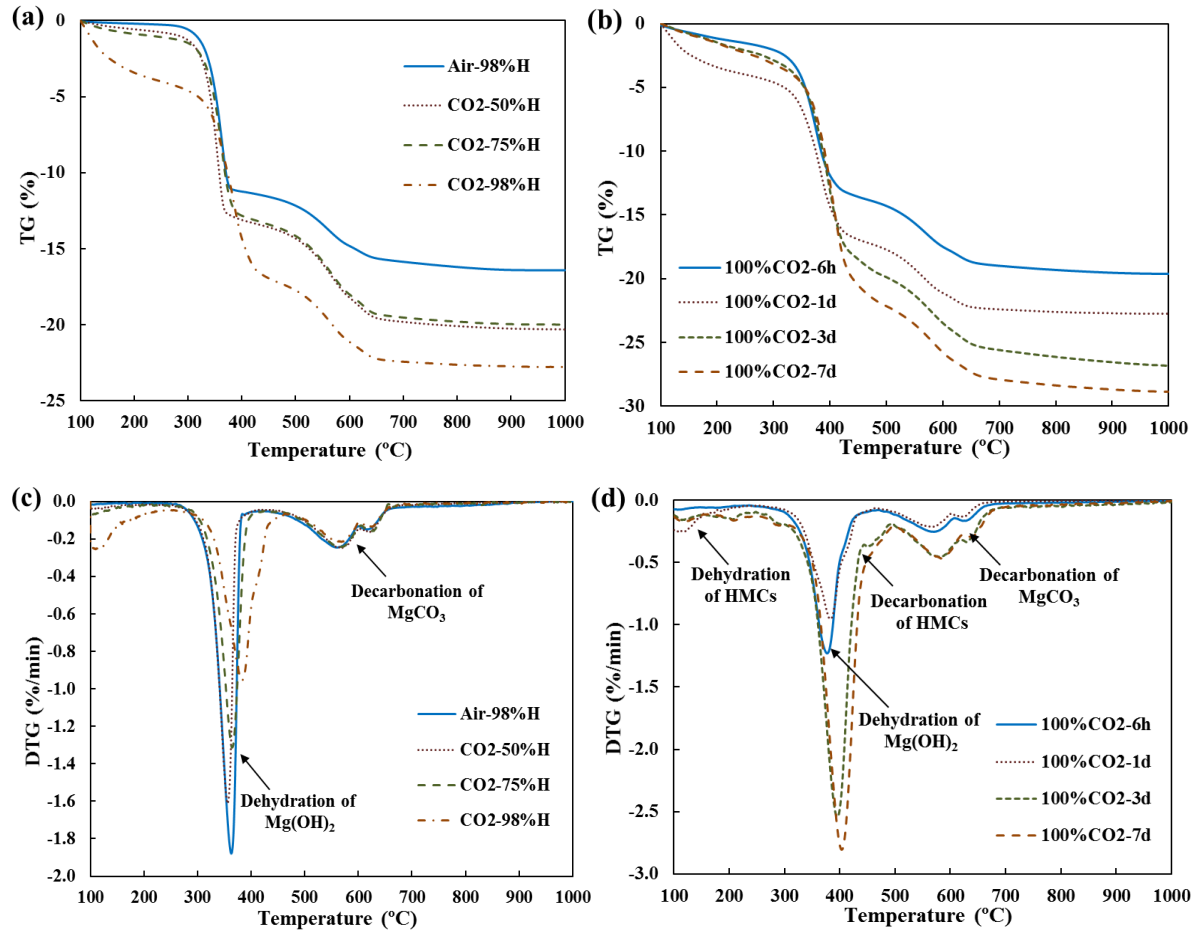


Figure 2. TGA of MC pastes: (a) TG curves of 1-d cured pastes as a function of curing environment and humidity; (b) TG curves of pastes at cured at 100% CO_2 and 98% humidity for different durations; (c) DTG curves corresponding to (a); (d) DTG curves corresponding to (b). (HMCs: hydrated magnesium carbonates).

The degree of carbonation in MC samples as a function of CO_2 curing time (at 98% humidity) is shown in Figure 2b&d. The content of newly formed HMCs in 6-h CO_2 samples was negligible, reflecting the low carbonation degree (i.e., the degree of the transformation of $\text{Ca}(\text{OH})_2$ and $\text{Mg}(\text{OH})_2$ into CaCO_3 , MgCO_3 and HMCs) in the early term. However, after 1-d CO_2 curing, the peak at 370 °C was shifted to a higher temperature. The mass loss of HMCs

reached 11.0 wt% and 14.2 wt% in 3-d and 7-d CO₂ cured samples, respectively. Therefore, sufficient curing time is essential for continued carbonation under the flow-through curing situation where both MgO hydration and CO₂ diffusion are time-dependent processes.

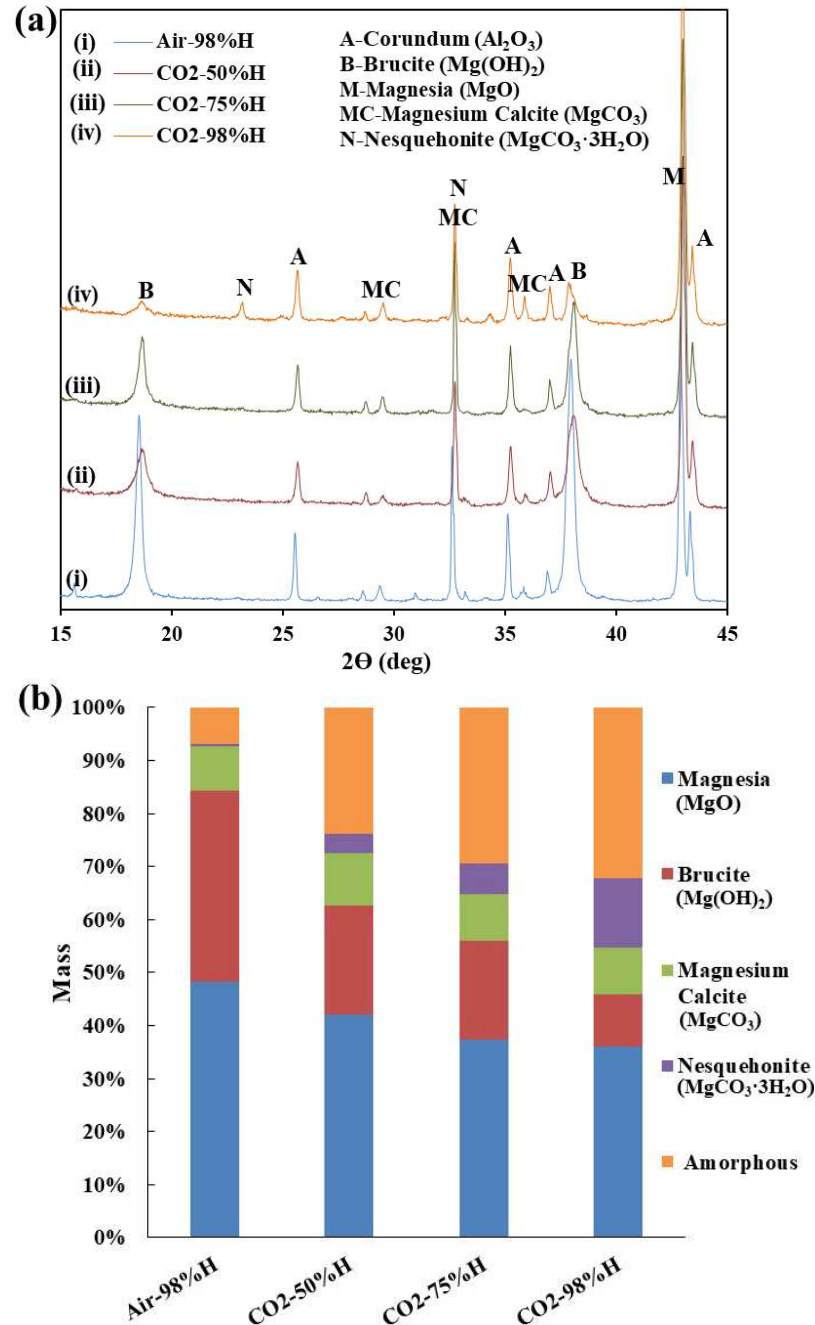


Figure 3. X-ray diffractograms (a) and Q-XRD analysis (b) of MC pastes cured for 1 day under air and CO₂ curing, with various relative humidities as marked.

The XRD diffractograms (Figure 3a) illustrate that a remarkable peak of brucite ($\text{Mg}(\text{OH})_2$) at $18.7^\circ 2\theta$ existed in 1-d air cured samples. The Q-XRD results (Figure 3b) further indicate that there was 36.1 wt% of $\text{Mg}(\text{OH})_2$ content and 48.2 wt% of unreacted MgO in the air cured samples. After 1-d CO_2 curing, the contents of both $\text{Mg}(\text{OH})_2$ and MgO decreased whereas the contents of MgCO_3 , nesquehonite ($\text{MgCO}_3 \cdot 3\text{H}_2\text{O}$), and amorphous phase (e.g., poorly-crystalline $\text{Mg}(\text{OH})_2$, MgCO_3 , and HMCs) increased, which agreed with the TGA results. In particular, for the samples with 98% humidity CO_2 curing, a new peak due to nesquehonite appeared at $23.2^\circ 2\theta$. The XRD results provide further evidence that high relative humidity (98%) is a favourable condition for CO_2 curing of MC-based materials under flow-through conditions.

Figure 4 shows that MC blocks, after 6-h air curing, had a low compressive strength (3.74 MPa), whereas the strength reached 17.6 MPa after 1-d air curing, and gradually increased with curing time due to continued MgO hydration. In the CO_2 cured samples, there was marginal enhancement of strength after 6-h CO_2 curing compared to the air-cured samples. This proved that 6-h curing was insufficient for CO_2 diffusion and further carbonation under the non-pressurised flow-through conditions, although accelerated carbonation has previously been shown to be nearly complete under higher-pressure CO_2 within 2-h of curing [34]. After 1-d CO_2 curing, the compressive strength of MC samples significantly increased, and after 7-d CO_2 curing at 98% humidity, it was 3.8 times higher than that of the 1-d air cured samples. These results demonstrate that MC pastes can be carbonated to generate abundant HMCs, as indicated by the TGA and Q-XRD results (Figure 2 and 3), for strength enhancement even in the non-pressurised flow-through curing system.

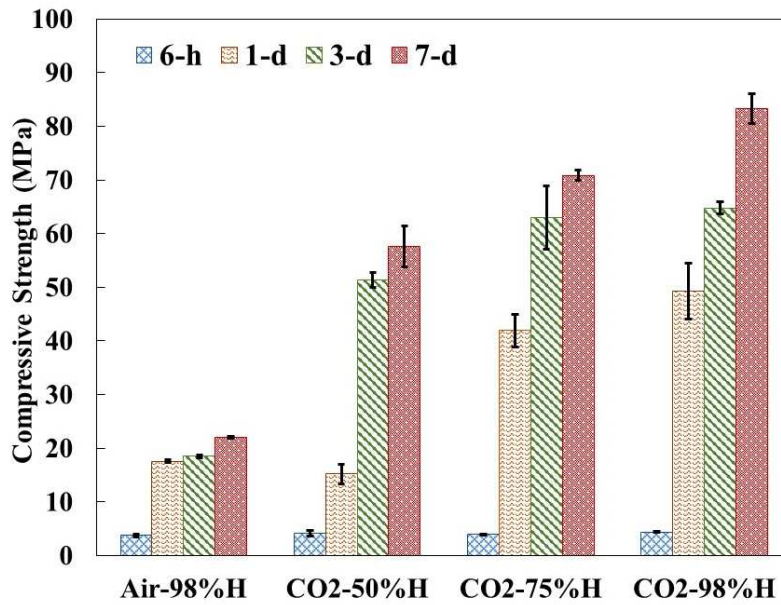


Figure 4. Compressive strength of MC pastes under air and CO₂ curing, with various relative humidities as marked.

3.1.2 BC Pastes

The TG and DTG curves of the 1-d cured BC pastes are illustrated in Figure 5a&c. From Figure 5c, 3.46 wt.% mass loss at 370 °C (equivalent to 11.7 wt.% Mg(OH)₂) and 1.04 wt.% mass loss at 410 °C (equivalent to 4.27 wt.% Ca(OH)₂) were observed in the 1-d air cured samples. By comparison, the Ca(OH)₂ peaks diminished and CaCO₃ peaks intensified after 1-d CO₂ curing, while Mg(OH)₂ was partially transformed into HMCs. Among the different relative humidity conditions tested, low humidity levels (50% and 75%) were favourable for the carbonation of BC pastes, which was distinct from the MC systems. In the BC system, the generation and dissolution of Ca(OH)₂ was much faster than Mg(OH)₂, thus, the CO₂ diffusion rate became the major limiting factor determining the overall rate of carbonation. As the CO₂ diffusion coefficient in water is 4 to 5 orders-of-magnitude lower than in air [35], low humidity levels (50% and 75%) facilitated CO₂ diffusion and increased the overall carbonation rate of the BC pastes.

Under 50% humidity, 6-h CO₂ curing significantly promoted the transformation from Ca(OH)₂ to CaCO₃, however, it had little effect on the carbonation of Mg(OH)₂. This reflects that CO₂ preferentially reacted with Ca to generate CaCO₃. One of the major reasons is that the ΔG of CaCO₃ generation (-73.0 kJ mol⁻¹) is lower than that of MgCO₃ generation (-30.2 kJ mol⁻¹) [34]. In addition, the dissolution and hydration of tricalcium silicate (C₃S) was much faster than that of reactive MgO in the BC system, thus the Ca(OH)₂ content was higher than the Mg(OH)₂ content at early age. After the consumption of Ca(OH)₂, Mg(OH)₂ was partially carbonated into HMCs after 1-d CO₂ curing, and then Mg(OH)₂ and HMCs were gradually transformed into MgCO₃, yet the content of hydrates and carbonates were similar in the 3-d and 7-d CO₂ cured samples.

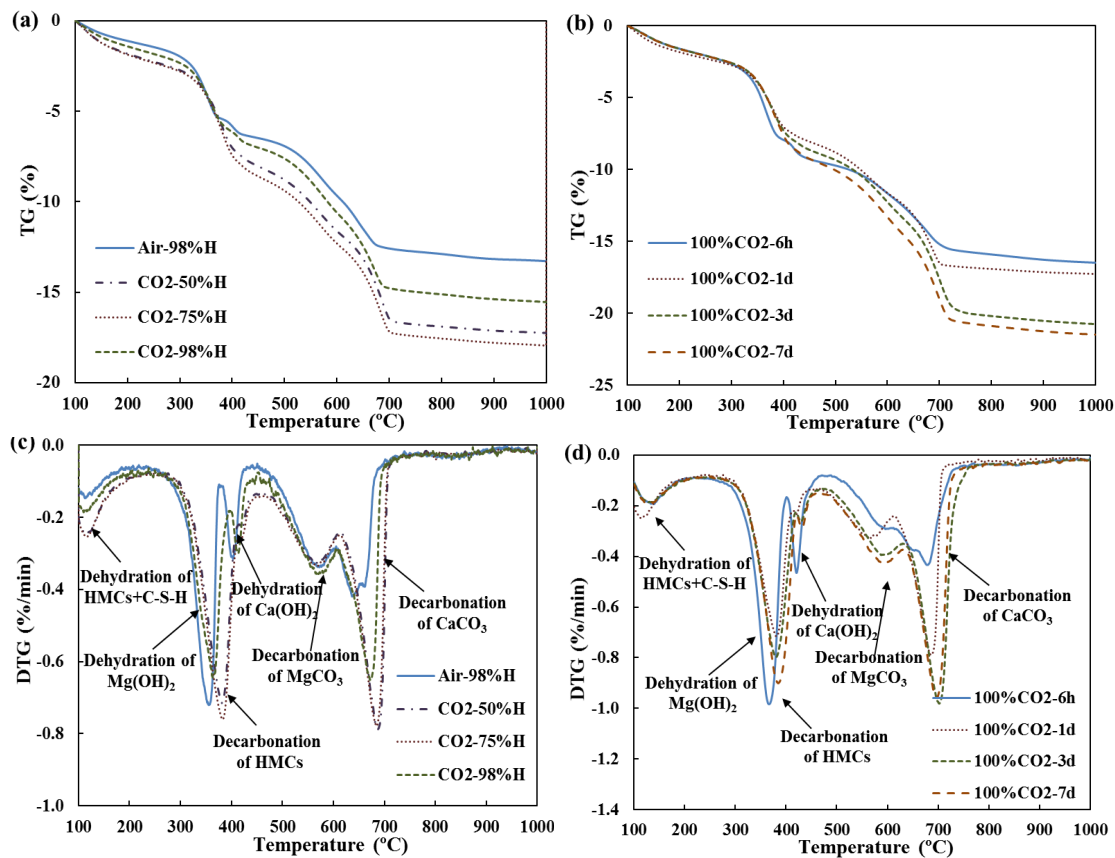


Figure 5. TGA of BC pastes: (a) TG curves of 1-d cured pastes as a function of curing environment and humidity; (b) TG curves of pastes at cured at 100% CO₂ and 50% humidity for different durations; (c) DTG curves corresponding to (a); (d) DTG curves corresponding to (b). (BC: binary cement; C-S-H: calcium silicate hydrate; HMCs: hydrated magnesium carbonates).

296

297 The Q-XRD results (Figure 6b) show that there were large quantities of unreacted MgO (34.8
298 wt%), C₃S (16.5 wt%), and C₂S (11.2 wt%) in the 1-d air cured samples. The 1-d CO₂ curing
299 effectively boosted the hydration and carbonation of raw materials to generate carbonates (e.g.,
300 CaCO₃). The Q-XRD results confirm that Ca(OH)₂ was preferentially carbonated during 1-d
301 CO₂ curing. In the early stage (1-d), the BC samples with 50% humidity CO₂ curing showed
302 the highest carbonation degree.

303

304 As shown in Figure 7, the compressive strength of BC blocks under 6-h air curing was only
305 0.67 MPa, while 6-h CO₂ curing enhanced the strength to 4.03 MPa. The carbonation rate in
306 the BC system was faster than in MC system due to the higher activity of Ca²⁺ in BC. After 1-
307 d CO₂ curing, all the carbonated samples were stronger than the 7-d air cured samples. The
308 strength of BC samples reached as high as 61.5 MPa after 7-d CO₂ curing. Among the samples,
309 50% humidity facilitated the early strength development of BC samples by accelerated
310 carbonation whereas 98% humidity promoted the later stage (7-d) strength development by
311 continued hydration and carbonation. Humidity as a key factor determining the rate of
312 carbonation can be adjusted at different stages of curing under the flow-through conditions
313 tested here, providing an interesting route to practical process optimisation.

314

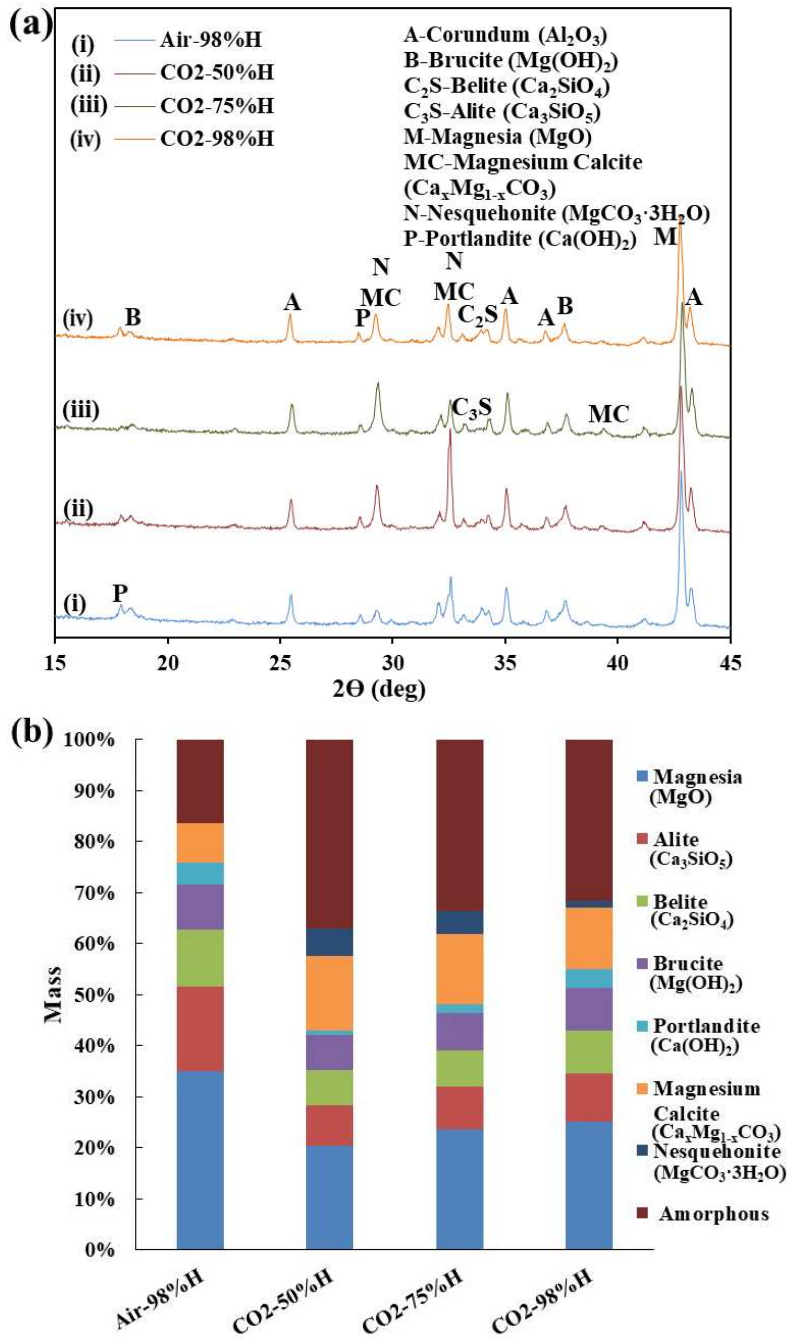


Figure 6. XRD diffractograms (a) and Q-XRD analysis (b) of 1-d cured BC pastes with different humidities

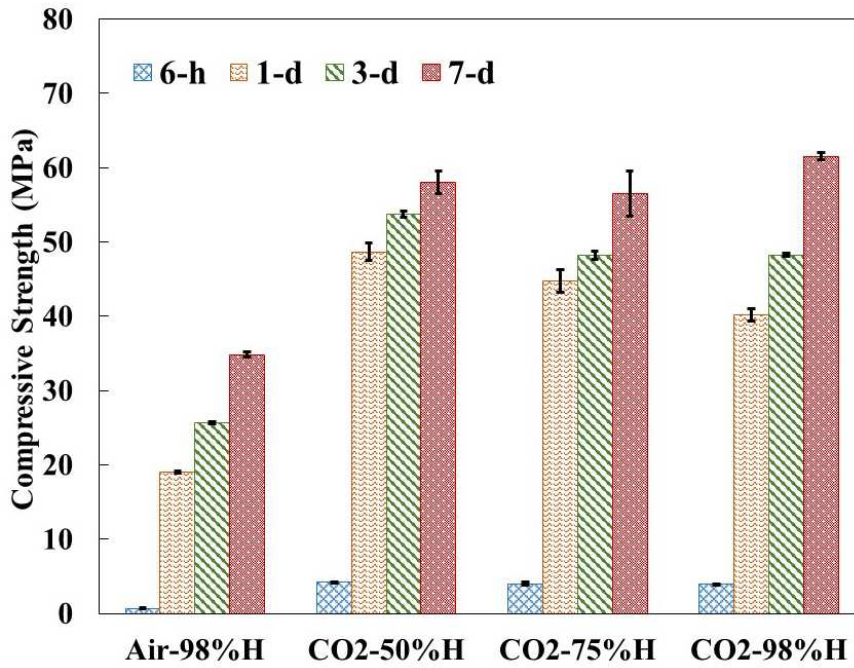


Figure 7. Compressive strengths of BC pastes under air and CO₂ curing with various humidities.

3.2 Efficiency of Various CO₂ Concentrations in Accelerated Carbonation

3.2.1 MC Pastes

As illustrated by the measured TG curves (Figure 8), the mass loss of all the carbonated samples was larger than the values for corresponding air cured samples (0% CO₂). After 1-d CO₂ curing, samples that had been subjected to different CO₂ concentrations showed similar weight drops in TG due to decarbonation at 570 °C (5.15 wt%) and 630 °C (1.30 wt%). However, compared to air cured samples, the peak at 370 °C was enlarged and shifted to 390 °C, especially for 70% CO₂ and 100% CO₂ samples. The broad peak between 100 °C and 300 °C also increased in 70% CO₂ and 100% CO₂ samples. These results suggest that the transformation of Mg(OH)₂ into HMCs was insignificant in the low CO₂ concentration (10% and 40%) samples while it was remarkable in the high CO₂ concentration (70% and 100%) samples. The degree of carbonation in 10% CO₂ samples increased with curing time (Figure 8b). Compared to 1-d CO₂ curing, the mass loss peak shifted from 370 °C to 390 °C after 3-d CO₂ curing (Figure 8d). The total weight drop of 7-d 10% CO₂ cured samples (22.8 wt%) was comparable to that of 1-d

100% CO₂ cured samples (22.7 wt%) (Figure 8b). Therefore, a relatively low concentration of CO₂ (e.g., 10%) under the flow-through curing conditions could still accelerate the carbonation of MC samples, and extended CO₂ curing effectively enhanced the carbonation degree.

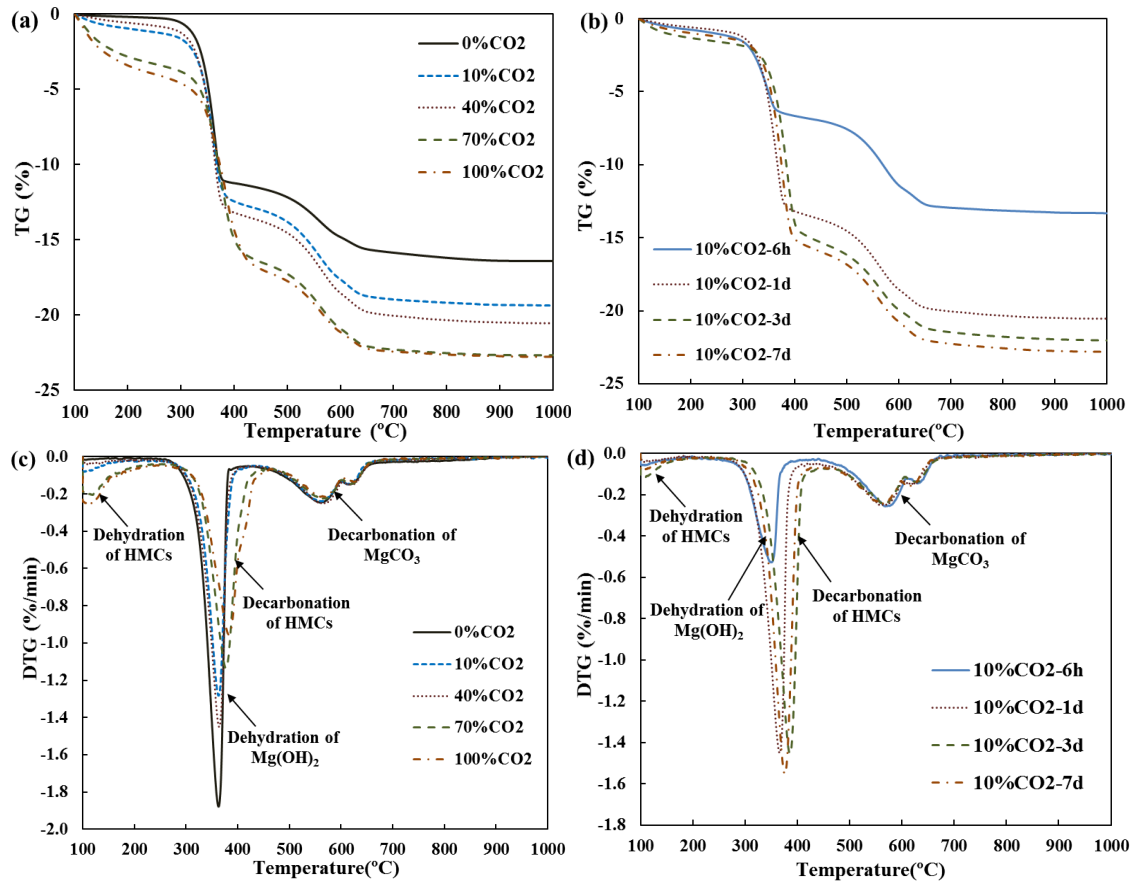


Figure 8. TGA of MC pastes: (a) TG curves of 1-d pastes as a function of CO₂ concentrations; (b) TG curves of pastes at cured at 10% CO₂ for different durations; (c) DTG curves corresponding to (a); (d) DTG curves corresponding to (b).

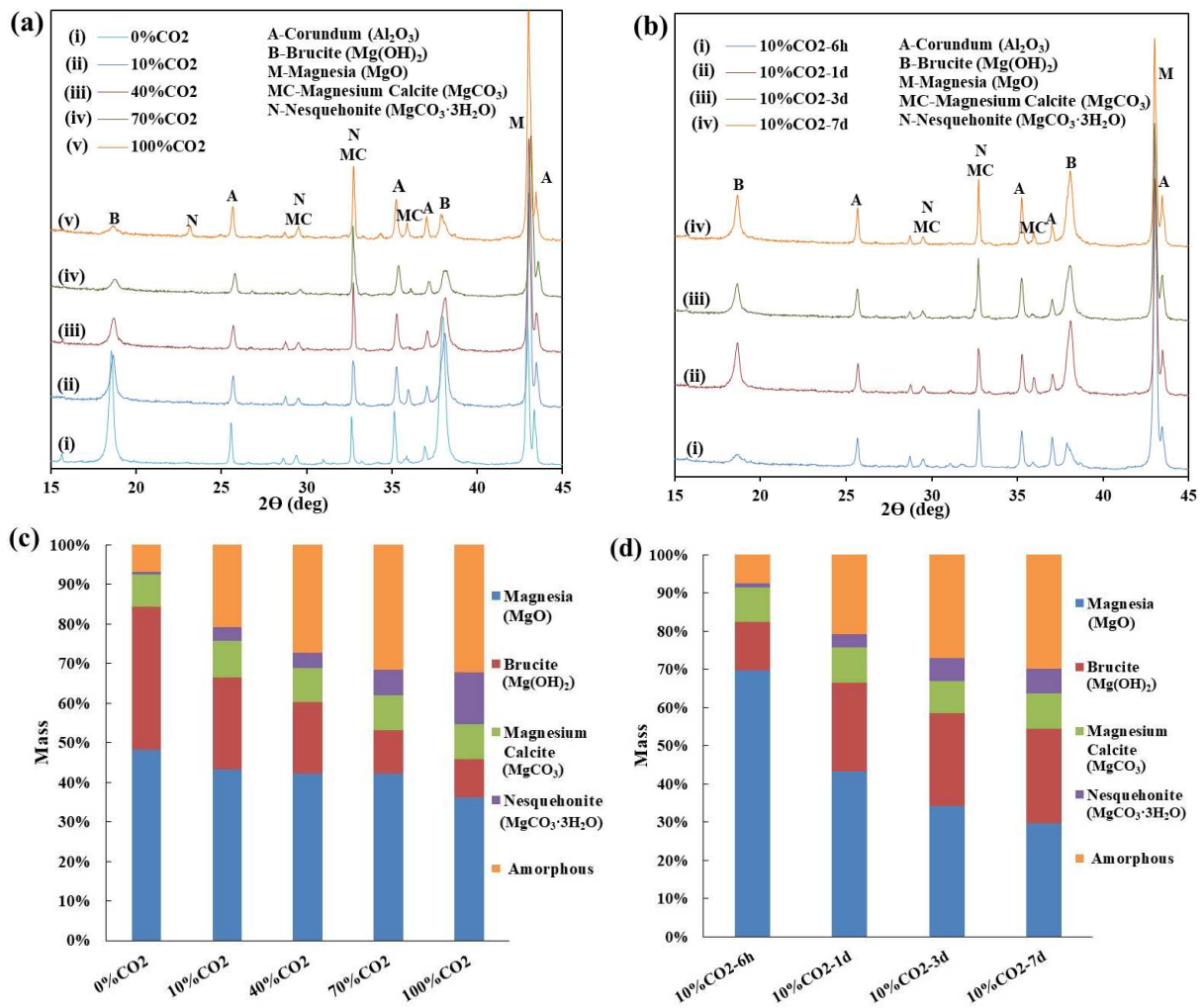


Figure 9. XRD diffractograms and Q-XRD analysis of MC pastes with different CO₂ concentrations and curing time: (a) XRD diffractograms of 1-d cured pastes with different CO₂ concentrations; (b) XRD diffractograms of pastes cured at 10% CO₂ concentration with different curing times; (c) Q-XRD analysis of 1-d cured pastes with different CO₂ concentrations; (d) Q-XRD analysis of pastes cured at 10% CO₂ concentration with different curing times.

Figure 9a illustrates that the XRD peak due to Mg(OH)₂ at 18.7° 2θ gradually decreased with increasing CO₂ concentration, whereas the content of MgCO₃ increased. In samples exposed to 100% CO₂, the peaks of nesquehonite appeared at 23.4° and 34.5° 2θ. The Q-XRD results further suggested that a high content of amorphous phase (approximately 31.2%) existed in 70% and 100% CO₂ cured samples, and HMCs were the dominant components of amorphous phase based on the TGA results. From Figure 9b&d, the content of MgCO₃ and amorphous HMCs in 10% CO₂ samples continually increased with curing time. The amorphous content

reached 30.2% after 7-d curing at 10% CO₂, which is further evidence that low-concentration CO₂ and sufficient curing time can still promote carbonation of MC products.

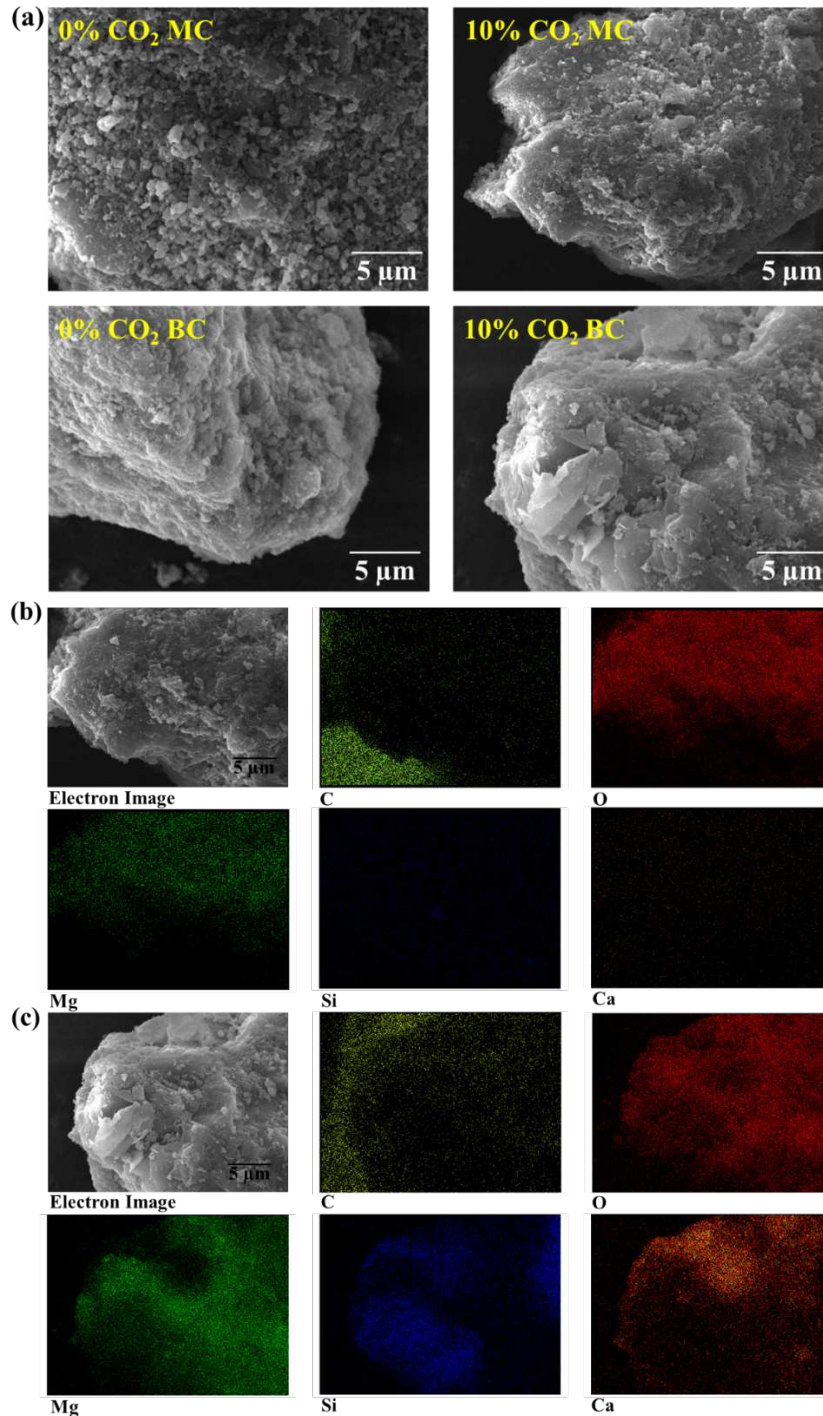


Figure 10. SEM images and elemental mapping of MC and BC samples: (a) SEM image of 1-d 0% CO₂ and 10% CO₂ cured MC and BC samples, (b) element mapping of 1-d 10% CO₂ cured MC samples, (c) element mapping of 1-d 10% CO₂ cured BC samples.

As illustrated in SEM images (Figure 10a), 1-d air (0% CO₂) cured MC samples had a rough surface with a large number of spherical particles, which may be unreacted MgO particles [36]. By comparison, 1-d 10% CO₂ cured MC samples showed a dense structure, suggesting favourable MC hydration and carbonation. Elemental mapping (Figure 10b) showed that Mg and O were the predominant elements and only a low content of C existed in 1-d 10% CO₂ cured samples. Therefore, under low-concentration CO₂ curing conditions, a long time CO₂ curing is required to achieve a high degree of carbonation.

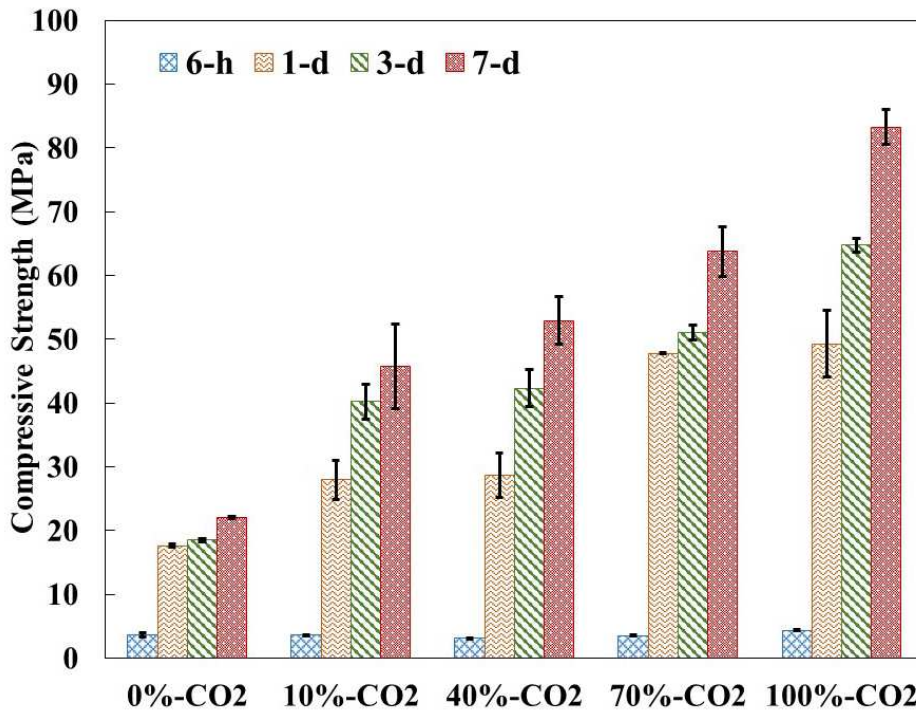


Figure 11. Compressive strengths of MC pastes under CO₂ curing with various CO₂ concentrations.

Figure 11 shows that after 6-h CO₂ curing, all the MC blocks showed comparable compressive strengths (3.74-4.41 MPa). After 1-d CO₂ curing, the differences in compressive strength were significant among different CO₂ cured samples. The 1-d 10% CO₂ cured samples showed higher strength than 7-d air cured samples, and strength increased with the increase of CO₂

concentration because of the favourable carbonation as indicated by the TGA and Q-XRD results (Figure 8 and 9). It should be noted that extended 10% CO₂ curing (7-d) yielded similar strengths to 1-d 100% CO₂ cured samples. These findings demonstrate that a low CO₂ concentration gas (e.g., industrial exhaust) could be used to accelerate carbonation of MC-based materials, although it needs a relatively long curing time compared to 100% CO₂ curing.

3.2.2 BC Pastes

Figure 12a illustrates that the mass loss of 1-d carbonated BC samples increased with an increase of CO₂ concentration, and that the Ca(OH)₂ in BC systems was preferentially carbonated into CaCO₃. The obvious peaks of Ca(OH)₂ could be observed for the lower-CO₂ cured samples, whereas Ca(OH)₂ peaks nearly disappeared and Mg(OH)₂ was partially transformed into HMCs and MgCO₃ in 100% CO₂ cured samples (Figure 12c). The contents of carbonates increased with CO₂ curing time. The extent of calcite decomposition measured by TG for 10%-CO₂ cured samples increased from 4.8 wt% (6-h curing) to 9.0 wt% (7-d curing). The peak of Mg(OH)₂ (370 °C) was also shifted to a temperature indicative of HMCs (390 °C) after 7-d CO₂ curing (Figure 12d). Thus, long-term curing at low concentration CO₂ curing could also accelerate the carbonation of BC.

As shown in Figure 13a&c, with the increase of CO₂ concentration the content of Ca(OH)₂ in 1-d cured BC samples gradually decreased, however, Mg(OH)₂ content was maintained at approximately 8.6%, except in 100% CO₂ cured samples, suggesting that only Ca(OH)₂ was partially carbonated in the early stages. From Figure 13b&d, the contents of Ca(OH)₂ and Mg(OH)₂ in 10% CO₂ cured samples continually decreased with increasing curing time, while the contents of calcite and amorphous phase accordingly increased. After 7-d curing at 10% CO₂, the contents of calcite and amorphous phase (C-S-H, calcium aluminate hydrates,

amorphous HMCs, poorly crystalline carbonates, etc.) reached 13.5% and 36.9%, respectively, which were also comparable to the contents of these phases in 1-d 100% CO₂ cured BC samples.

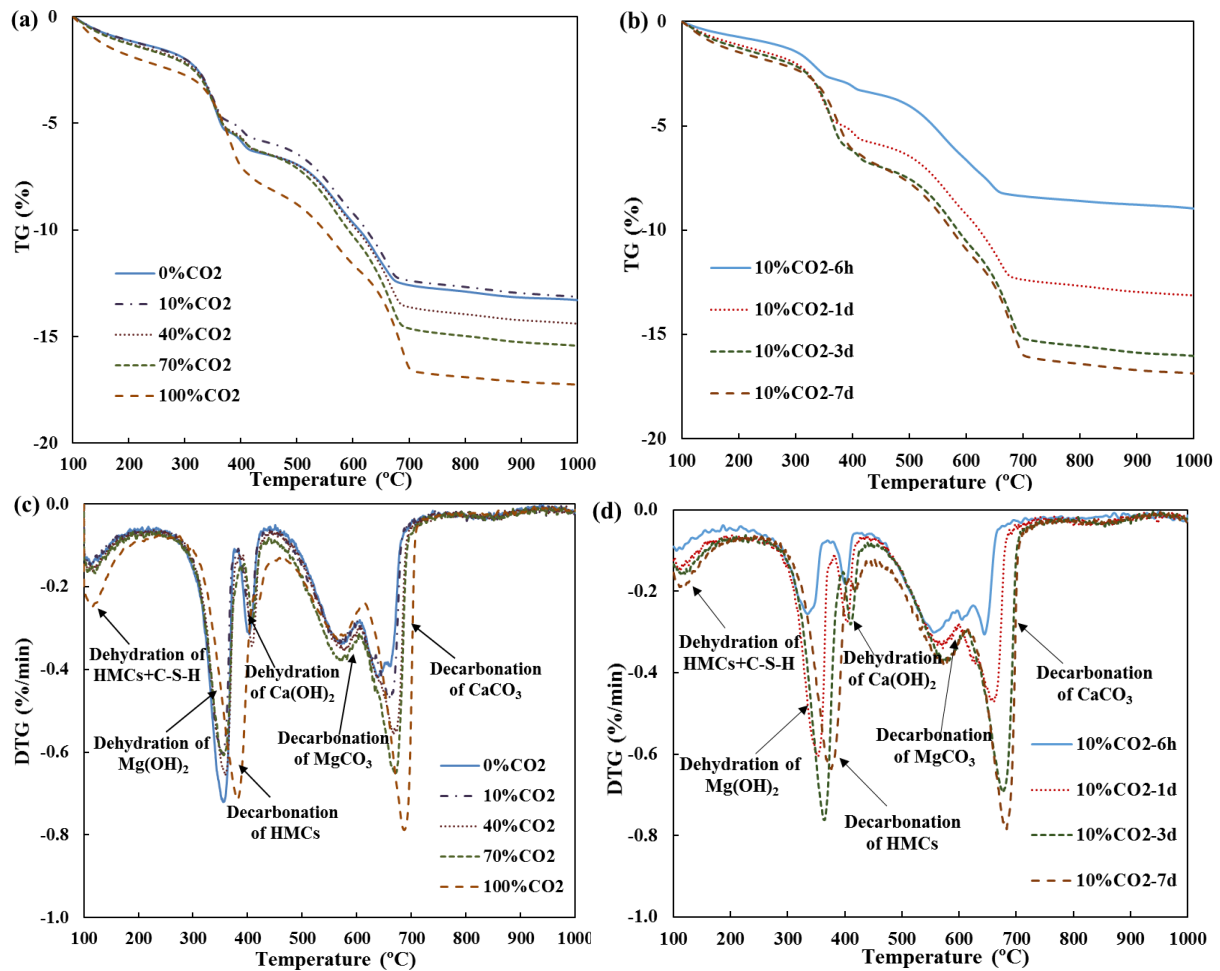


Figure 12. TGA of BC pastes: (a) TG curves of 1-d pastes as a function of CO₂ concentrations; (b) TG curves of pastes at cured at 10% CO₂ for different durations; (c) DTG curves corresponding to (a); (d) DTG curves corresponding to (b).

From SEM imaging (Figure 10a), 1-d air cured BC samples had a rough surface but the spherical particles on the surface were not remarkable. In contrast to the MC samples, most of MgO particles in the BC samples might be enclosed by PC hydrates (e.g., C-S-H gel) [37]. After 1-d 10% CO₂ curing, a smooth and dense surface could be observed for BC samples. Elemental mapping (Figure 10c) illustrated that 1-d 10% CO₂ cured BC samples have a higher

content of carbon than the corresponding MC samples, and the carbon overlapped with the Ca-rich areas. This provides further evidence that CO_2 reacted with Ca^{2+} preferentially due to the relatively high solubility and reactivity of $\text{Ca}(\text{OH})_2$. Therefore, the PC in the BC system played an important role in promoting the early-term carbonation in low- CO_2 concentration condition.

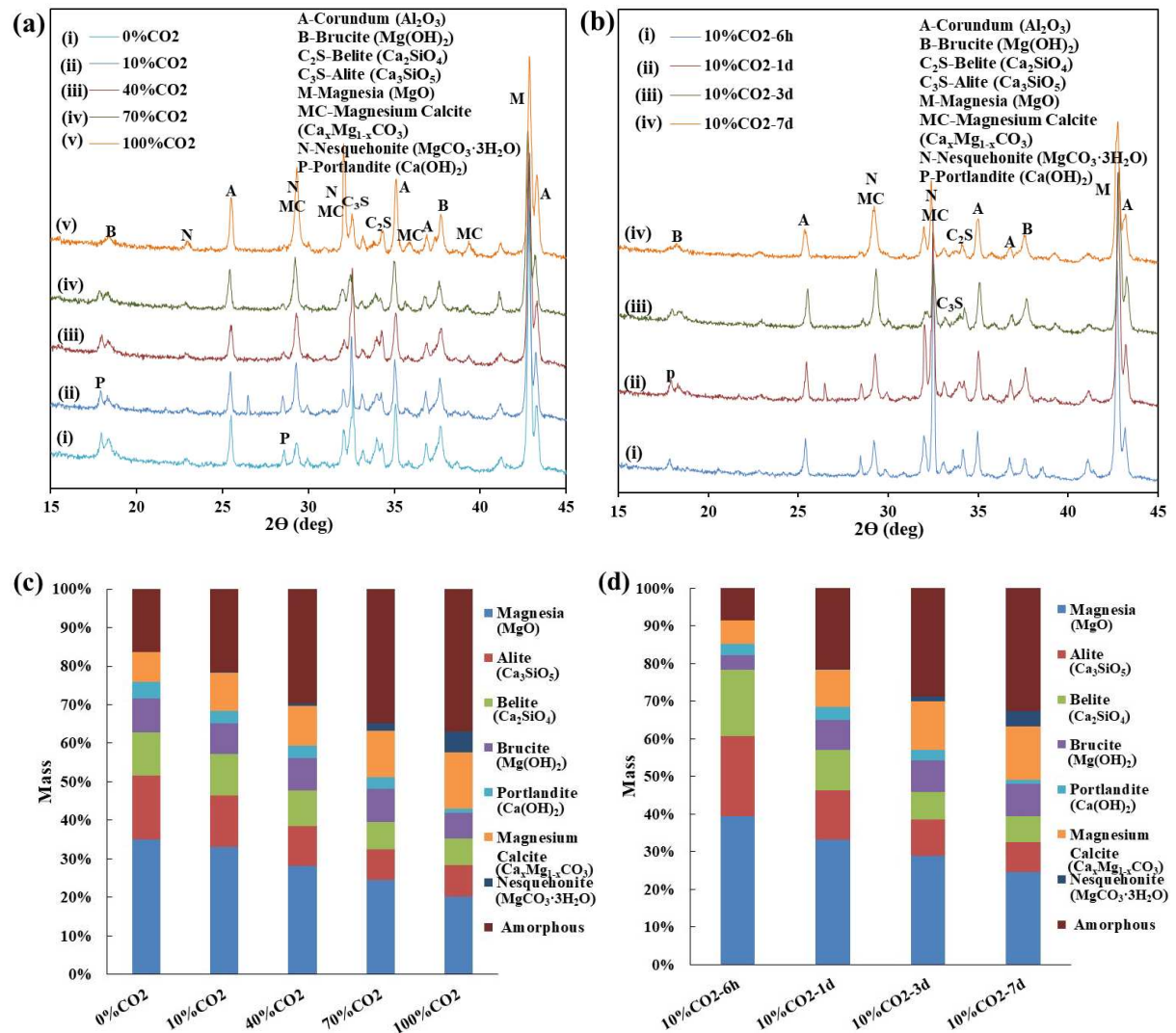


Figure 13. XRD diffractograms and Q-XRD analysis of BC pastes with different CO_2 concentrations and curing times: (a) XRD diffractograms of 1-d cured pastes with different CO_2 concentrations; (b) XRD diffractograms of pastes cured at 10% CO_2 concentration with different curing times; (c) Q-XRD analysis of 1-d cured pastes with different CO_2 concentrations; (d) Q-XRD analysis of pastes cured at 10% CO_2 concentration with different curing times.

As shown in Figure 14, BC samples with high-concentration CO_2 curing presented higher

compressive strengths at different curing durations due to their higher carbonation rate. However, the lower CO₂ concentration curing still effectively accelerated carbonation. Compared to 7-d air cured samples, the 7-d 10% CO₂ cured samples showed 31.8% enhancement of compressive strength, which gave comparable strength with 1-d 100% CO₂ cured samples. Therefore, low CO₂ concentration gas under flow-through conditions is also effective for accelerating the carbonation of BC-based materials.

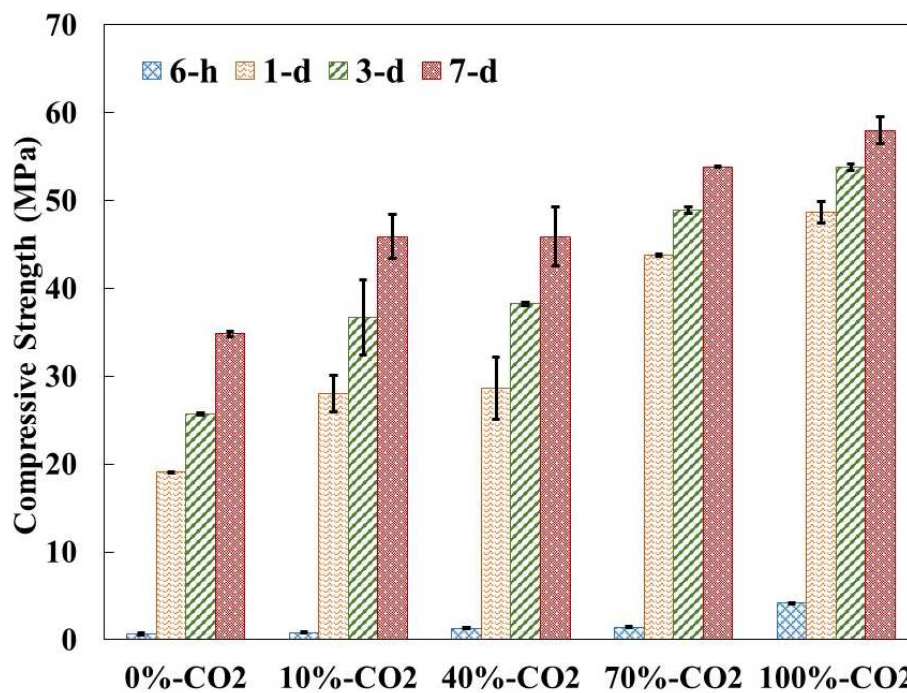


Figure 14. Compressive strength of BC pastes cured under CO₂ with various CO₂ concentrations.

3.3 Effect of Acids on Accelerated Carbonation

The TG results (Figure 15) indicate that the mass loss of hydrates and carbonates of 1-d CO₂ cured MC samples significantly reduced in the presence of H₂SO₄ and HNO₃ as representative acids that may be observed in flue gases. The carbonation of the MC samples was significantly inhibited by the acidic conditions. As the acidities of H₂SO₄ and HNO₃ are stronger than H₂CO₃, carbonates could not displace SO₄²⁻ and NO₃⁻ from the MC samples as the stronger acids reacted preferentially with the solid alkaline phases [38]. The sulphation and nitration are

irreversible processes [39]. It should be noted that the molar concentration of H_2SO_4 tested here was 5.83 times higher than the value of HNO_3 based on an investigation in power plant exhaust (in Supplementary Information). From Figure 15c, compared to acid-free MC samples, the mass loss in TG attributed to HMCs decomposition in acid-incorporated samples significantly reduced, especially for the H_2SO_4 -MC samples. Thus, in actual application, a high concentration of SO_2 in the exhaust may have a remarkable inhibitive effect on MC carbonation.

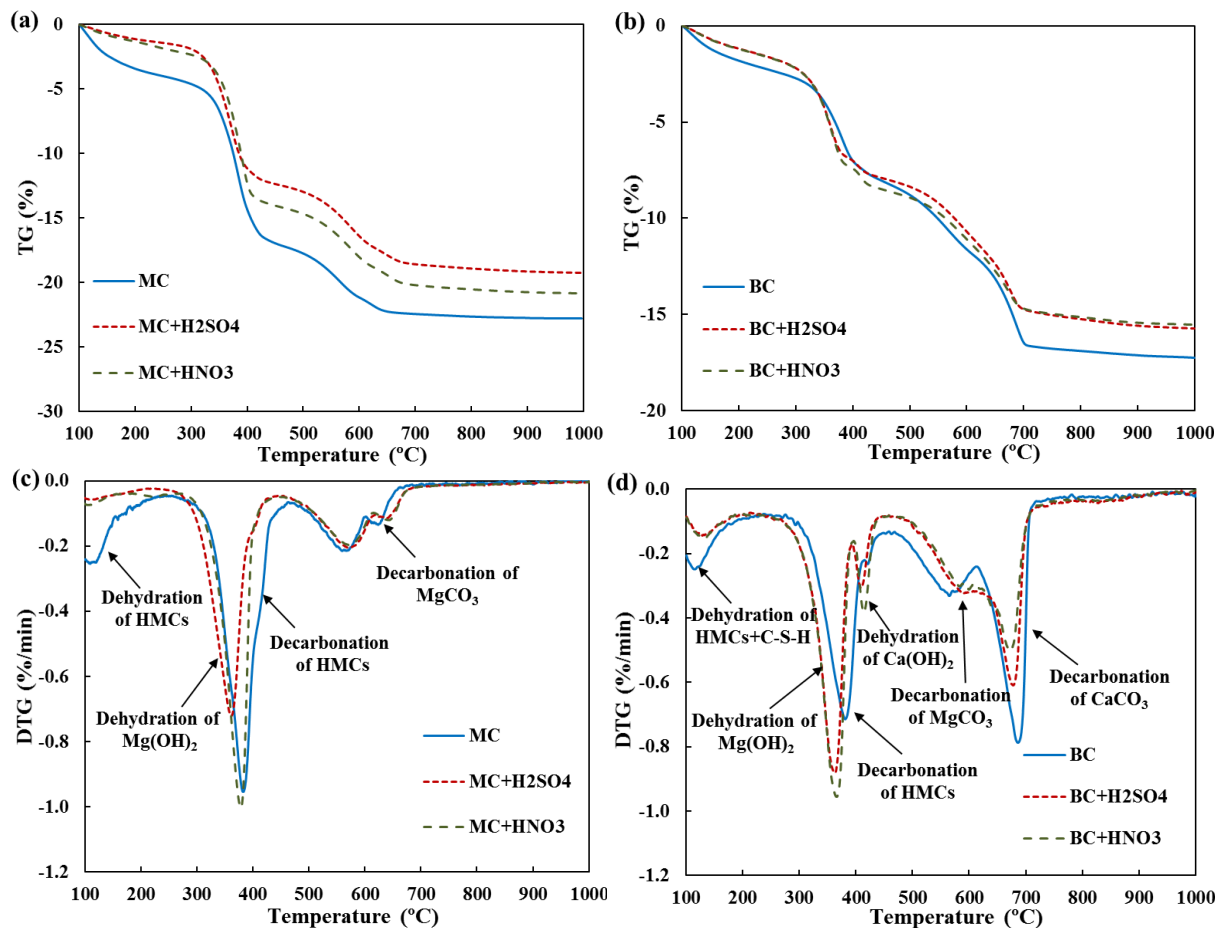


Figure 15. TGA of 1-d 100% CO_2 cured pastes with H_2SO_4 and HNO_3 addition: (a) TG curves of MC pastes with addition of acids; (b) TG curves of BC pastes with addition of acids; (c) DTG curves corresponding to (a); (d) DTG curves corresponding to (b).

477

478 In the TG analysis of the 1-d CO₂ cured BC system (Figure 15b&d), the presence of H₂SO₄
479 and HNO₃ resulted in an 11% reduction in the mass loss of the hydrates and carbonates,
480 respectively, which was lower than the reduction in the MC system. This suggests that BC
481 samples had better compatibility with acids compared to MC samples. The high concentration
482 of H₂SO₄ and low concentration of HNO₃ had a similar inhibitory effect on carbonation in the
483 BC system. The H₂SO₄ may react with Ca(OH)₂ to form CaSO₄, which is one of the
484 components in PC (Table 1). Thus, PC in the BC system may to some degree be able to
485 compensate for the adverse effect of H₂SO₄.

486

487 As shown in Figure 16, compared to acid-free CO₂ cured MC samples, the acid-incorporated
488 samples contained a higher content of uncarbonated Mg(OH)₂, particularly for the H₂SO₄
489 samples. Q-XRD analyses further indicated that the presence of H₂SO₄ and HNO₃ reduced the
490 content of nesquehonite by 90.3% and 84.7%, respectively, and also the amorphous content
491 decreased. In the BC system, the acids also resulted in the increase of unreacted raw materials
492 and decrease of carbonates and hydrates (crystalline or amorphous phases). In particular, the
493 presence of H₂SO₄ in BC samples consumed Ca(OH)₂ and decreased the content of calcite.

494

495 From Figure 17, the incorporation of acids decreased the compressive strength of 1-d air cured
496 MC samples by approximately 37.8% due to its inhibitory effect on the hydrates formation.
497 For CO₂ cured samples, the addition of H₂SO₄ and HNO₃ led to 64.0% and 44.5% strength
498 reduction, respectively. This suggests that acids significantly inhibited the carbonation of MC,
499 especially for high-concentration H₂SO₄, which was in accordance with TGA and XRD results.
500 Conversely, the incorporation of H₂SO₄ and HNO₃ showed a negligible effect on the strength
501 reduction in the air cured BC system, but reduced the strength of CO₂ cured BC samples by

40.8% and 39.8%, respectively. Hence, compared to the MC system, the BC system had a better compatibility with acids. To ensure effective accelerated carbonation, desulphurisation and acid gas neutralisation in the exhaust gas should be considered before employing this gas as a flow-through CO₂ curing source for MC and BC systems.

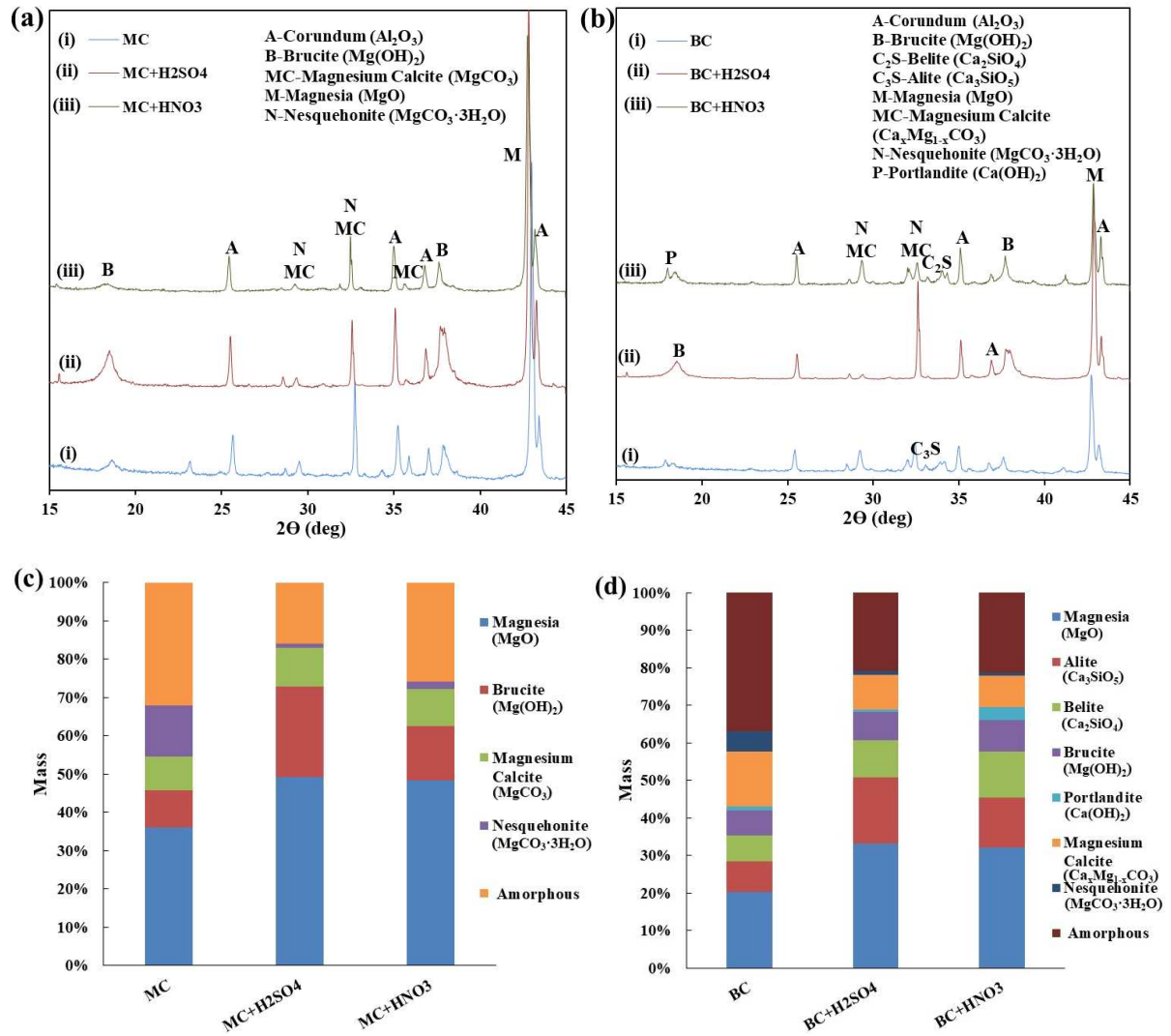


Figure 16. XRD diffractograms and Q-XRD analysis of 1-d 100% CO₂ cured pastes with H₂SO₄ and HNO₃ addition: (a) XRD diffractograms of MC pastes with addition of acids; (b) XRD diffractograms of BC pastes with addition of acids; (c) Q-XRD analysis of MC pastes with addition of acids; (d) Q-XRD analysis of BC pastes with addition of acids.

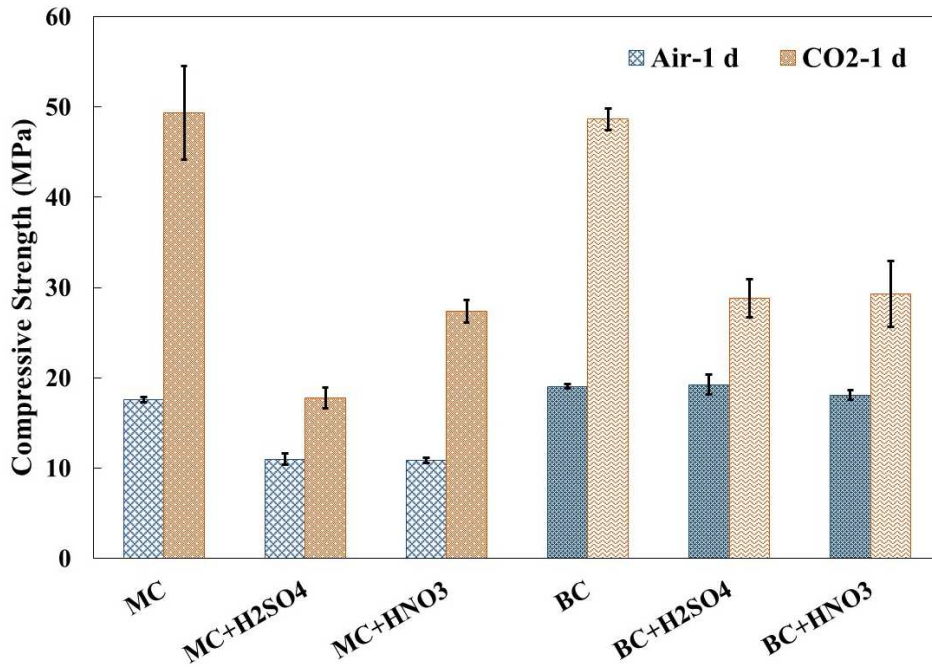


Figure 17. Compressive strengths of 1-d air and 100% CO₂ cured MC and BC samples with addition of acids.

4. Conclusions

This study investigated the accelerated carbonation of low-carbon reactive MgO cement and ordinary Portland cement blends under flow-through CO₂ gas conditions. The experimental results showed that flow-through CO₂ curing at a relatively low concentration (simulated industrial exhaust) effectively accelerated carbonation and enhanced compressive strength of single MgO cement (MC) pastes and binary cement (BC) pastes. High relative humidity (98%) was favourable for CO₂ curing of the MC system due to the high water consumption of MC for the generation and dissolution of Mg(OH)₂, whereas low humidity (50%) was an optimal parameter for BC paste carbonation. The addition of Portland cement (PC) into the BC system boosted early-term carbonation rate due to the rapid formation and dissolution of Ca(OH)₂. Despite the lower carbonation rate at 10% CO₂ concentration, the carbonation degree and compressive strength of 7-d 10% CO₂ cured samples were comparable to the values obtained for 1-d 100% CO₂ cured samples. Nevertheless, the presence of acids replicating the acid gases in industrial exhausts had inhibitory effects on the carbonation and hydration of MC pastes. By

comparison, the PC included in the BC system have a better compatibility with SO_4^{2-} and partly relieved the inhibitory effect. In future studies, the effect of NO_2 and SO_2 from the exhaust gas on the carbonation and hydration of cement-based materials should be further evaluated, and the flow-through curing system should be optimised to enhance the recovery rate of CO_2 from the exhaust gas. Overall, this study demonstrated that low-carbon MgO -based cement can be a promising material for sequestering and utilising CO_2 from industrial exhausts to promote the development of negative-emission technologies.

Acknowledgement

The authors appreciate the financial support from the Hong Kong Research Grants Council (PolyU 15223517 and E-PolyU503/17) for this study.

References

- [1] K.L. Scrivener, V.M. John, E.M. Gartner, Eco-efficient cements: Potential economically viable solutions for a low- CO_2 cement-based materials industry, *Cem. Concr. Res.* 114 (2018) 2–26.
- [2] N.T. Dung, C. Unluer, Development of MgO concrete with enhanced hydration and carbonation mechanisms, *Cem. Concr. Res.* 103 (2018) 160–169.
- [3] Y. Geng, Z. Wang, L. Shen, J. Zhao, Calculating of CO_2 emission factors for Chinese cement production based on inorganic carbon and organic carbon, *J. Clean. Prod.* 217 (2019) 503–509.
- [4] L. Wang, K. Yu, J.S. Li, D.C.W. Tsang, C.S. Poon, J.C. Yoo, K. Baek, S. Ding, D. Hou, J.G. Dai, Low-carbon and low-alkalinity stabilization/solidification of high-Pb contaminated soil, *Chem. Eng. J.* 351 (2018) 418–427.

556 [5] A. Al-Tabbaa, Reactive magnesia cement, in: *Eco-Efficient Concrete*. Woodhead
557 Publishing (2013) 523–543.

558 [6] T. Zhang, X. Liang, C. Li, M. Lorin, Y. Li, L.J. Vandeperre, C.R. Cheeseman, Control of
559 drying shrinkage in magnesium silicate hydrate (M-S-H) gel mortars, *Cem. Concr. Res.* 88
560 (2016) 36–42.

561 [7] H. Dong, E.H. Yang, C. Unluer, F. Jin, A. Al-Tabbaa, Investigation of the properties of
562 MgO recovered from reject brine obtained from desalination plants, *J. Clean. Prod.* 196 (2018)
563 100–108.

564 [8] S.A. Walling, J.L. Provis, Magnesia-Based Cements: A Journey of 150 Years, and Cements
565 for the Future?, *Chem. Rev.* 116 (2016) 4170–4204.

566 [9] Y. Tan, H. Yu, Y. Li, W. Bi, X. Yao, The effect of slag on the properties of magnesium
567 potassium phosphate cement, *Constr. Build. Mater.* 126 (2016) 313–320.

568 [10] L. Wang, L. Chen, D.W. Cho, D.C.W. Tsang, J. Yang, D. Hou, K. Baek, H.W. Kua, C.S.
569 Poon, Novel synergy of Si-rich minerals and reactive MgO for stabilisation/solidification of
570 contaminated sediment, *J. Hazard. Mater.* 365 (2019) 695–706.

571 [11] L. Wang, L. Chen, D.C.W. Tsang, H.W. Kua, J. Yang, Y.S. Ok, S.M. Ding, D.Y. Hou,
572 C.S. Poon, The roles of biochar as green admixture for sediment-based construction products.
573 *Cem. Concr. Compos.* 104 (2019) 103348.

574 [12] C. Kuenzel, F. Zhang, V. Ferrándiz-Mas, C.R. Cheeseman, E.M. Gartner, The mechanism
575 of hydration of MgO-hydromagnesite blends, *Cem. Concr. Res.* 103 (2018) 123–129.

576 [13] L. Wang, I.K.M. Yu, D.C.W. Tsang, K. Yu, S. Li, C. Sun Poon, J.G. Dai, Upcycling wood
577 waste into fibre-reinforced magnesium phosphate cement particleboards, *Constr. Build. Mater.*
578 159 (2018) 54–63.

579 [14] L. Mo, F. Zhang, M. Deng, F. Jin, A. Al-Tabbaa, A. Wang, Accelerated carbonation and
580 performance of concrete made with steel slag as binding materials and aggregates, *Cem. Concr.*
581 *Compos.* 83 (2017) 138–145.

582 [15] F. Cao, M. Miao, P. Yan, Hydration characteristics and expansive mechanism of MgO
583 expansive agents, *Constr. Build. Mater.* 183 (2018) 234–242.

584 [16] B.J. Zhan, D.X. Xuan, C.S. Poon, C.J. Shi, Effect of curing parameters on CO₂ curing of
585 concrete blocks containing recycled aggregates, *Cem. Concr. Compos.* 71 (2016) 122–130.

586 [17] C. Shi, Z. Wu, Z. Cao, T.C. Ling, J. Zheng, Performance of mortar prepared with recycled
587 concrete aggregate enhanced by CO₂ and pozzolan slurry, *Cem. Concr. Compos.* 86 (2018)
588 130–138.

589 [18] N.T. Dung, C. Unluer, Carbonated MgO concrete with improved performance: The
590 influence of temperature and hydration agent on hydration, carbonation and strength gain,
591 *Cem. Concr. Compos.* 82 (2017) 152–164.

592 [19] S.A. Walling, J.L. Provis, A discussion of the papers “Impact of hydrated magnesium
593 carbonate additives on the carbonation of reactive MgO cements” and “Enhancing the
594 carbonation of MgO cement porous blocks through improved curing conditions”, by C. Unluer
595 & A. Al-Tabbaa, *Cem. Concr. Res.* 79 (2016) 424–426.

596 [20] M. Fernández Bertos, S.J.R. Simons, C.D. Hills, P.J. Carey, A review of accelerated
597 carbonation technology in the treatment of cement-based materials and sequestration of CO₂.,
598 *J. Hazard. Mater.* 112 (2004) 193–205.

599 [22] L. Mo, F. Zhang, D.K. Panesar, M. Deng, Development of low-carbon cementitious
600 materials via carbonating Portland cement–fly ash–magnesia blends under various curing
601 scenarios: a comparative study, *J. Clean. Prod.* 163 (2017) 252–261.

602 [21] L. Pu, C. Unluer, Durability of carbonated MgO concrete containing fly ash and ground
603 granulated blast-furnace slag, *Constr. Build. Mater.* 192 (2018) 403–415.

- [23] L. Mo, D.K. Panesar, Effects of accelerated carbonation on the microstructure of Portland cement pastes containing reactive MgO, *Cem. Concr. Res.* 42 (2012) 769–777.
- [24] S. Ruan, C. Unluer, Influence of mix design on the carbonation, mechanical properties and microstructure of reactive MgO cement-based concrete, *Cem. Concr. Compos.* 80 (2017) 104–114.
- [25] R. Zhang, D.K. Panesar, Mechanical properties and rapid chloride permeability of carbonated concrete containing reactive MgO, *Constr. Build. Mater.* 172 (2018) 77–85.
- [26] L. Wang, S.S. Chen, D.C.W. Tsang, C.S. Poon, J.G. Dai, CO₂ curing and fibre reinforcement for green recycling of contaminated wood into high-performance cement-bonded particleboards, *J. CO₂ Util.* 18 (2017) 107–116.
- [27] R. Zhang, N. Bassim, D.K. Panesar, Characterization of Mg components in reactive MgO - Portland cement blends during hydration and carbonation, *J. CO₂ Util.* 27 (2018) 518–527.
- [28] W. Shen, L. Cao, Q. Li, Z. Wen, J. Wang, Y. Liu, R. Dong, Y. Tan, R. Chen, Is magnesia cement low carbon? Life cycle carbon footprint comparing with Portland cement, *J. Clean. Prod.* 131 (2016) 20–27.
- [29] L. Wang, L. Chen, D.C.W. Tsang, J.S. Li, T.L.Y. Yeung, S. Ding, C.S. Poon, Green remediation of contaminated sediment by stabilization/solidification with industrial by-products and CO₂ utilization, *Sci. Total Environ.* 631–632 (2018) 1321–1327.
- [30] I. Taniguchi, T. Yamada, Low energy CO₂ capture by electrodialysis, in: *Energy Proced.* (2017) 1615–1620.
- [31] D. Xuan, B. Zhan, C.S. Poon, A maturity approach to estimate compressive strength development of CO₂-cured concrete blocks, *Cem. Concr. Compos.* 85 (2018) 153–160.
- [32] BS EN 12390, Testing Hardened Concrete Compressive Strength of Test Specimens. British Standards Institution, London, UK (2009).

- [33] L. Han, X. Li, J. Bai, F. Xue, Y. Zheng, C. Chu, Effects of flow velocity and different corrosion media on the in vitro bio-corrosion behaviours of AZ31 magnesium alloy, *Mater. Chem. Phys.* 217 (2018) 300–307.
- [34] L. Wang, S.S. Chen, D.C.W. Tsang, C.S. Poon, K. Shih, Recycling contaminated wood into eco-friendly particleboard using green cement and carbon dioxide curing, *J. Clean. Prod.* 137 (2016) 861–870.
- [35] C. Unluer, A. Al-Tabbaa, Enhancing the carbonation of MgO cement porous blocks through improved curing conditions, *Cem. Concr. Res.* 59 (2014) 55–65.
- [36] L. Wang, L. Chen, D.W. Cho, D.C.W. Tsang, J. Yang, D. Hou, K. Baek, H.W. Kua, C.S. Poon, Novel synergy of Si-rich minerals and reactive MgO for stabilisation/solidification of contaminated sediment, *J. Hazard. Mater.* (2019) 695–706.
- [37] D.K. Panesar, L. Mo, Properties of binary and ternary reactive MgO mortar blends subjected to CO₂ curing, *Cem. Concr. Compos.* 38 (2013) 40–49.
- [38] H. Chen, C. Zhao, Q. Ren, Feasibility of CO₂/SO₂ uptake enhancement of calcined limestone modified with rice husk ash during pressurized carbonation, *J. Environ. Manage.* 93 (2012) 235–244.
- [39] A. Coppola, A. Esposito, F. Montagnaro, G. De Tommaso, F. Scala, P. Salatino, Effect of exposure to SO₂ and H₂O during the carbonation stage of fluidised bed calcium looping on the performance of sorbents of different nature, *Chem. Eng. J.* (2018).

Supplementary Information

Calculation of H₂SO₄ and HNO₃ dosage in MC and BC pastes

Based on our field investigation, the typical CO₂, SO₂, and NO₂ concentrations in thermal power plant exhaust are 7-12%, 3500-4500 mg Nm⁻³, and 400-600 mg Nm⁻³, respectively. In this study, we assumed that CO₂, SO₂, and NO₂ concentrations from the thermal power plant are **10%**, 4000 mg Nm⁻³, and 500 mg Nm⁻³, respectively; these **SO₂ and NO₂** concentrations are equivalent to **0.14% and 0.024%** in the exhaust, respectively.

According to TGA results, the **CO₂ absorption extent is 4%** in the MC paste (CO₂ concentration of 100%, humidity of 98%). The reaction between acid gas and alkaline paste is a diffusion-controlled reaction. Here, we assume that diffusion rates of acid gas are the same as the rate of diffusion of CO₂ gas. Thus, the absorption extent of acid gas depends on the concentration of acid gas in the exhaust.

We can calculate the dosage of H₂SO₄ and HNO₃ as follows:

$$m_{H_2SO_4} = 4\% \frac{0.14}{10} \times \frac{98}{44} \times 100\% = 0.125\% g$$

$$m_{HNO_3} = 4\% \frac{0.024}{10} \times \frac{63}{44} \times 100\% = 0.0137\% g$$

Therefore, **H₂SO₄ (0.125 wt% of paste)** and **HNO₃ (0.0137 wt% of paste)** are added in the specified mixtures, respectively.

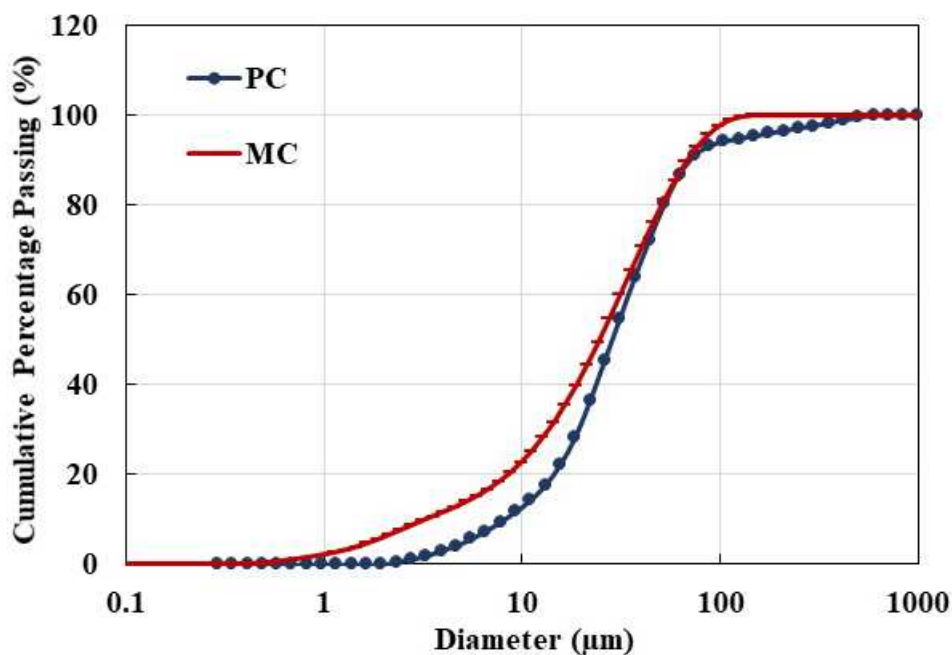


Figure S1. Particle size distribution of raw PC and MC.

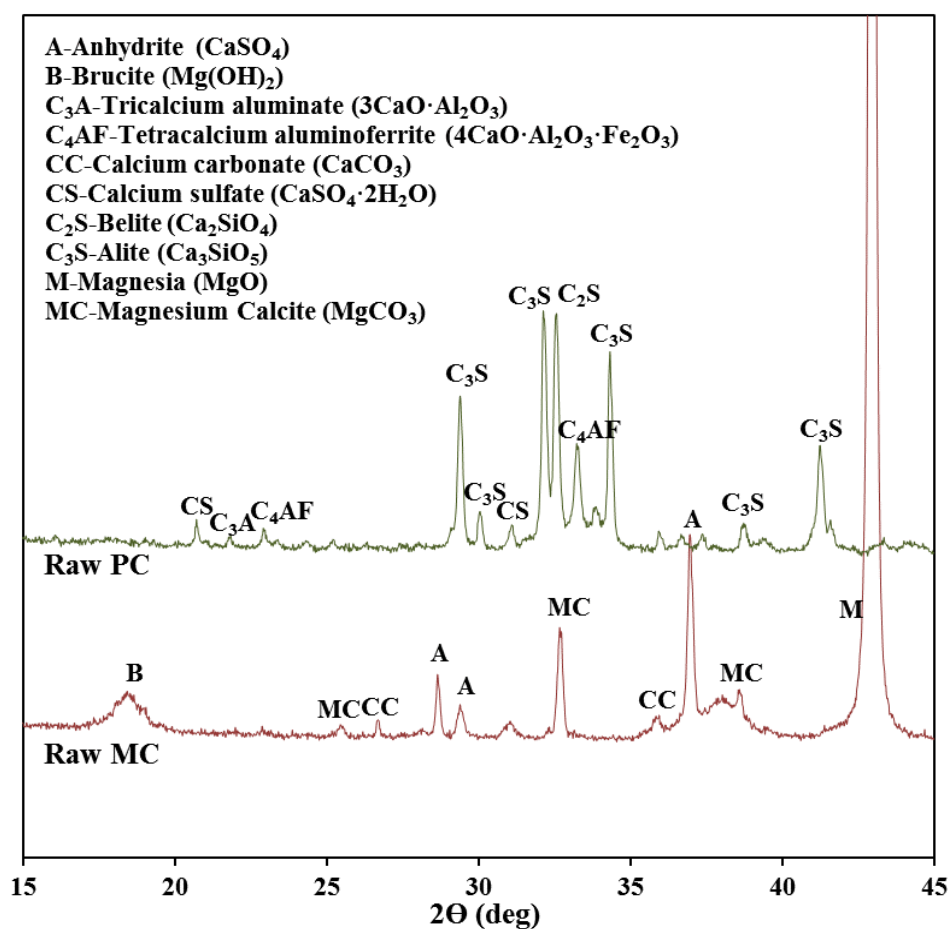


Figure S2. XRD diffractograms of raw PC and MC.

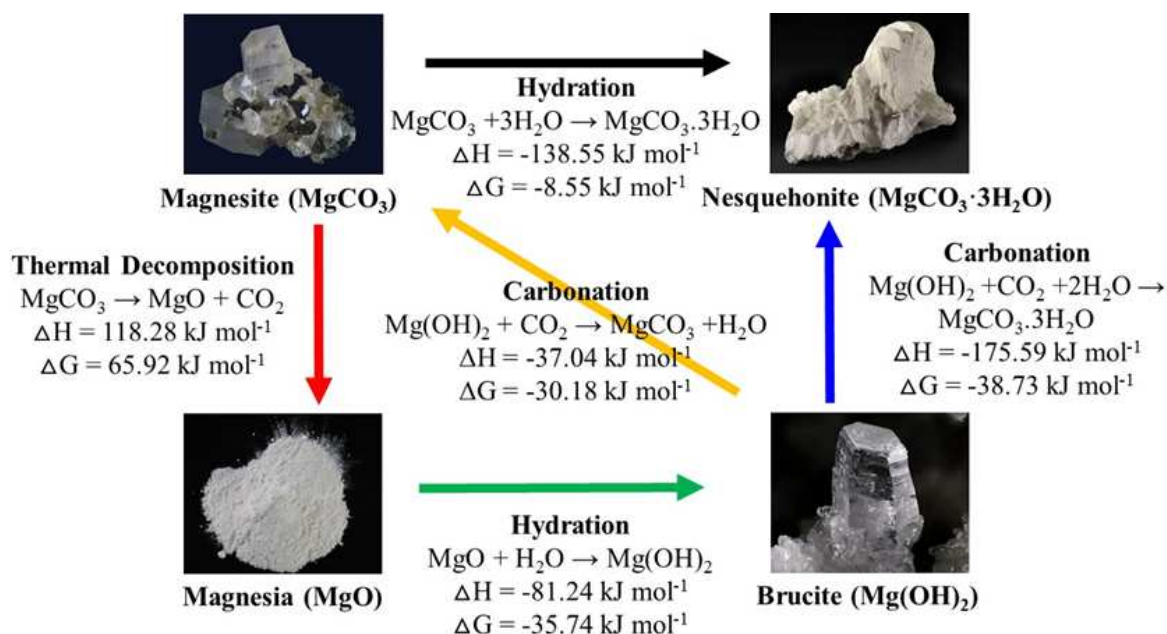


Figure S3. Thermodynamic reactions of the family of magnesium oxides/carbonates (Wang et al., 2016). Copyright Elsevier.

Reference:

Wang, L., Chen, S.S., Tsang, D.C.W., Poon, C.S., Shih K.M., 2016. Recycling contaminated wood into eco-friendly particleboard using green cement and carbon dioxide curing. J. Clean. Prod. 137, 861-870.

ELSEVIER LICENSE TERMS AND CONDITIONS

Sep 19, 2019

This Agreement between Mr. liang chen ("You") and Elsevier ("Elsevier") consists of your license details and the terms and conditions provided by Elsevier and Copyright Clearance Center.

License Number	4672520469961
License date	Sep 19, 2019
Licensed Content Publisher	Elsevier
Licensed Content Publication	Journal of Cleaner Production
Licensed Content Title	Recycling contaminated wood into eco-friendly particleboard using green cement and carbon dioxide curing
Licensed Content Author	Lei Wang,Season S. Chen,Daniel C.W. Tsang,Chi-Sun Poon,Kaimin Shih
Licensed Content Date	Nov 20, 2016
Licensed Content Volume	137
Licensed Content Issue	n/a
Licensed Content Pages	10
Start Page	861
End Page	870
Type of Use	reuse in a journal/magazine
Requestor type	academic/educational institute
Intended publisher of new work	Elsevier
Portion	figures/tables/illustrations
Number of figures/tables/illustrations	1
Format	both print and electronic
Are you the author of this Elsevier article?	Yes
Will you be translating?	No
Original figure numbers	figures 1
Title of the article	Accelerated Carbonation of Reactive MgO and Portland Cement Blends Under Flowing CO ₂ Gas
Publication new article is in	Cement and Concrete Composites
Publisher of the new article	Elsevier
Author of new article	Lei Wang, Liang Chen, John L. Provis, Daniel C.W. Tsang, Chi-Sun Poon
Expected publication date	Jul 2019
Estimated size of new article (number of pages)	21
Requestor Location	Mr. liang chen ZS922, 9/F, Block Z, polyu

<https://s100.copyright.com/AppDispatchServlet>

1/6